Published in final edited form as:

FASEB J. 2020 June ; 34(6): 8493–8509. doi:10.1096/fj.201903133RR.

CHCHD10-regulated OPA1-mitofilin complex mediates TDP-43-induced mitochondrial phenotypes associated with Frontotemporal dementia

Tian Liu[1,2], **Jung-A A. Woo**[1,3], **Mohammed Zaheen Bukhari**[1,2], **Patrick LePochat**[1,2], **Ann Chacko**[1,2], **Maj-Linda B. Selenica**[5], **Yan Yan**[1,2], **Peter Kotsiviras**[1,2], **Sara Cazzaro Buosi**[1,2], **Xingyu Zhao**[1,2], **David E. Kang**[1,2,4,*]

[1]Byrd Alzheimer's Center & Research Institute, USF Health Morsani College of Medicine, Tampa, FL 33613, USA

[2]Department of Molecular of Medicine, USF Health Morsani College of Medicine, Tampa, FL 33613, USA

[3]Department of Molecular Pharmacology and Physiology, USF Health Morsani College of Medicine, Tampa, FL 33613, USA

[4]James A. Haley Veterans Administration Hospital, Tampa, FL 33612, USA

[5]Sanders-Brown Center on Aging, University of Kentucky, Lexington, KY 40536-0230

Abstract

Mutations in *CHCHD10,* a gene coding for a mitochondrial protein, are implicated in ALS-FTD spectrum disorders, which are pathologically characterized by TDP-43 accumulation. While both TDP-43 and CHCHD10 mutations drive mitochondrial pathogenesis, mechanisms underlying such phenotypes are unclear. Moreover, despite the disruption of the mitochondrial mitofilin protein complex at cristae junctions in patient fibroblasts bearing the CHCHD10^{S59L} mutation, the role of CHCHD10 variants in mitofilin-associated protein complexes in brain has not been examined. Here, we utilized novel CHCHD10 transgenic mouse variants (WT, R15L & S59L), TDP-43 transgenic mice, FTLD-TDP patient brains, and transfected cells to assess the interplay between CHCHD10 and TDP-43 on mitochondrial phenotypes. We show that CHCHD10 mutations disrupt mitochondrial OPA1-mitofilin complexes in brain, associated with impaired mitochondrial fusion and respiration. Likewise, CHCHD10 levels and OPA1-mitofilin complexes are significantly reduced in brains of FTLD-TDP patients and TDP-43 transgenic mice. In cultured cells, CHCHD10 knockdown results in OPA1-mitofilin complex disassembly, while TDP-43 overexpression also reduces CHCHD10, promotes OPA1-mitofilin complex disassembly via

*Correspondence and request for materials should be addressed to D.E.K. (dkang@usf.edu) or T.L. (tianliu@usf.edu).

Author contributions

Conceptualization: Tian Liu, David E. Kang; Methodology: Tian Liu, Jung-A A. Woo, David E. Kang; Formal analysis and investigation: Tian Liu, Jung-A A. Woo, Mohammed Zaheen Bukhari, Patrick LePochat, Ann Chacko, Yan Yan, Peter Kotsiviras, Sara Cazzaro Buosi, David E. Kang; Writing - original draft preparation: Tian Liu, David E. Kang; Writing - review and editing: Tian Liu, David E. Kang; Funding acquisition: David E. Kang; Resources: Tian Liu, Jung-A A. Woo, Maj-Linda B. Selenica, Xingyu Zhao, David E. Kang; Supervision: David E. Kang

Conflict of interest

The authors declare no competing interests.

CHCHD10, and impairs mitochondrial fusion and respiration, phenotypes that are rescued by wild type CHCHD10. These results indicate that disruption of CHCHD10-regulated OPA1-mitofilin complex contributes to mitochondrial abnormalities in FTLD-TDP and suggest that CHCHD10 restoration could ameliorate mitochondrial dysfunction in FTLD-TDP.

Keywords

CHCHD10; TDP-43; Frontotemporal dementia; OPA1; mitofilin

Introduction

Frontotemporal lobar degeneration (FTLD), a condition associated frontotemporal dementia (FTD), and amyotrophic lateral sclerosis (ALS) are progressive neurodegenerative diseases sharing multiple common genetic and pathological links. More than 95% of ALS and ~50% of FTD (FTLD-TDP variant) are pathologically characterized by the accumulation of TDP-43, which are typically seen as aggregated cytoplasmic TDP-43 inclusions mislocalized from the nucleus (1, 2). These cases invariably exhibit severe mitochondrial abnormalities (3–5), which are closely associated with TDP-43 pathology (6, 7). Indeed, recent studies indicate that the accumulation of TDP-43 in mitochondria of neurons induces mitochondrial dysfunction and synaptic damage (8–10). Specifically, TDP-43 is colocalized with mitochondria and reduces mitochondrial length by increasing mitochondrial fission, which leads to abnormalities in mitochondrial dynamics and transport (10, 11). Moreover, overexpression of wild type TDP-43 in transgenic mice shows increased levels of the activated mitochondrial fission proteins Dynamin related protein 1 (Drp1) and Fission1 (Fis1), reduced levels of fusion protein mitofusion1 (Mfn1), as well as fragmented and aggregated mitochondria (7). However, there remain significant gaps in the mechanistic understanding of TDP-43 in mitochondrial pathogenesis.

The cristae structure of mitochondria is formed from the folds created by the inner membrane, which provides an extended surface area allowing the localization of OXPHOS enzymes to produce adenosine triphosphate (ATP). The maintenance of cristae structure is regulated by an important protein complex called ‘mitochondria contact site and cristae organization system’ (MICOS), which is concentrated at cristae junctions (12). Mitofilin/Mic60, the key component of MICOS (13), is an inner membrane protein essential for maintaining mitochondrial cristae structure and respiration as well as cellular viability in response to stress (13–17). Mitofilin also interacts with Optic atrophy 1 (OPA1), an inner membrane GTPase best known for its role in mitochondrial fusion (18–20). OPA1 activity is regulated by proteolytic processing from transmembrane long forms (L-OPA1) to soluble short forms (S-OPA1) produced by mitochondrial proteases Oma1 and YME1L (21), and the interaction between OPA1 and mitofilin plays a key role in regulating both inner membrane fusion (18) and cristae integrity (22, 23).

The nuclear gene *Coiled-coil-helix-coiled-coil-helix domain containing 10* (*CHCHD10*) encodes a small 15-kDa mitochondrial protein, which is mutated in sporadic and familial FTD-ALS spectrum disorders (24–27). *CHCHD10* mutations are also associated with spinal

muscular atrophy Jokela type (SMAJ) (28) and Charcot-Marie-Tooth disease type 2 (CMT2) (29). CHCHD10 is recognized as an important mitochondrial protein regulating mitochondrial respiration as well as maintenance of mitochondrial genome and cristae structure (8, 24, 30). A previous study identified CHCHD10 as a component of MICOS, in which CHCHD10 physically interacts with the core protein mitofilin (31), and fibroblasts derived patients bearing the CHCHD10^{S59L} mutation exhibit impaired MICOS and disrupted cristae (31, 32). However, many important questions remain. For example, how do FTD/ALS-linked CHCHD10 mutations produce mitochondrial abnormalities in the central nervous system (CNS)? Do TDP-43-induced mitochondrial phenotypes converge on CHCHD10-dependent mechanisms? If so, what is the role of endogenous CHCHD10 in the CNS of human FTLD-TDP and mouse models of FTLD-TDP? Finally, can wild type CHCHD10 protect against TDP-43-induced mitochondrial damage? In this study, we utilized novel CHCHD10 transgenic mouse variants (WT, R15L & S59L), human TDP-43 (hTDP-43) transgenic mice, FTLD-TDP patient brains, and transfected cells to demonstrate that that CHCHD10 mediates TDP-43-induced mitochondrial phenotypes at least in part through disruption of OPA1-mitofilin complexes in the CNS.

Material and Methods

Ethics approval

All the experiments methods and protocols involving mice in this study were approved by Institutional Animal Care and Use Committee (IACUC) at the University of South Florida (USF), and all methods were performed in accordance with the relevant guidelines and regulations have also been approved by USF IACUC and Institutional Biosafety Committees (IBC).

Human brain samples

Frozen tissues from the frontal gyrus of FTLD-TDP and nondemented controls were obtained from Dr. Allan Levey and Dr. Marla Gearing at Emory Alzheimer's Disease Research Center (ADRC). Pathology-confirmed FTLD-TDP and nondemented control tissues were matched as closely as possible for sex, age, and APOE genotypes during the procurement phase by the Emory ADRC (P50 AG025688).

Mice

Wild type C57BL6 and hemizygous transgenic mice expressing CHCHD10-WT, CHCHD10-R15L, CHCHD10-S59L, or WT human TDP-43 (TAR4) were bred in the C57BL6 background. Water and food were supplied *ad libitum* with 12-hour light/dark cycle under standard vivarium conditions. TAR4 mice have previously been described (33). Briefly, the transgenic mice line was generated by using an mTUB expression vector with Thy-1 promoter expressing wild-type human TDP-43 (TARDBP, NM_007375) on the BI6/SJL background mice and bred with Ntg C57BL6/J background mice (33).

To develop transgenic mice expressing human CHCHD10 variants, we obtained the transgenic expression construct containing the mouse *PrP* promoter (MoPrP.Xho) from Dr. David Borchelt (University of Florida, FL, USA), which was previously used to generate the

widely used APP/PS1 (34), PS19 tauP301S (35), and -synuclein A53T (36) transgenic mice. We subcloned Flag-CHCHD10 (WT, R15L, & S59L) variants into the XhoI site of the MoPrP.Xho vector and verified the entire cDNA region by sequencing. Purified transgenic constructs were sent to the University of Utah Gene Targeting Core (Salk Lake City, Utah, USA) for injection into embryos. Each transgenic construct was microinjected into the pronuclei of at least 200 fertilized C57BL/6 embryos and implanted into the oviduct of pseudo-pregnant mice. From over 100 offspring born from multiple mothers per transgenic construct, genomic DNA from tails were isolated at the time of weaning and genotyped for the transgene by PCR (Supplemental Fig. S1a; representative gel) using the following primer sets specific for the human CHCHD10 transgene: forward primer, 5'–GCTCATGGCTCAGATGGCGAC–3' and reverser primer 5'-AGGGCAGGGAGCTCAGACCAT-3'. PCR-positive founders were bred with C57BL/6 mice for at least 3 generations to ascertain stable transmission of the transgene prior to determination of transgene expression profiles. Upon establishment of transgenic lines, CHCHD10 transgenes were amplified by PCR from genomic DNA, and the entire open reading frame was sequenced to confirm the presence of the intended transgene. To quantify transgenic CHCHD10 transcripts relative to the endogenous CHCHD10 transcript, total RNA isolated from non-transgenic and CHCHD10 transgenic mice (WT, R15L, & S59L) were subjected to qRT-PCR using primer sequences common to both mouse and human CHCHD10 mRNA: Set 1: forward primer 5'-CCCTGTGTGAGGGCTTCAGCGA-3', reverse primer 5'-TCAGGGCAGGGAGCTCAGACC-3'; Set 2: forward primer 5'-CCCCTGCAGATGGGGCCCTGC-3'; reverse primer 5'-TCAGGGCAGGGAGCTCAGACC-3'. Transgenic lines from CHCHD10-WT, CHCHD10-R15L, and CHCHD10-S59L strains with the closest transgenic protein and mRNA expression in brain were chosen for further experiments (Fig. 1b,c; Supplemental Fig. S1b–d).

Cell culture

HEK293T, Hela, and NIH3T3 cells were cultured in Dulbecco's modified Eagle's medium (DMEM, Thermo Scientific, MA, USA) supplemented with 10% fetal bovine serum (FBS) and 1% penicillin/streptomycin (P/S). Mouse cortical primary neurons from P0 pups were cultured in Neurobasal medium with 1 × B-27 supplement and 1 × L-Glutamine (Invitrogen, CA, USA) in humidified atmosphere (5% CO_2) at 37°C as previously described (8, 37).

DNA constructs, siRNAs, and lentivirus generation

P3X-Flag-CHCHD10-WT, P3X-Flag-CHCHD10-R15L and P3X-Flag-CHCHD10-S59L were described previously (8). OPA1-myc construct was obtained from Dr. Alexander M. van der Bliek (University of California, Los Angeles, CA, USA), and mito-dendra2 construct was obtained from Addgene (38). The siRNA duplexes (19 nt) targeting human CHCHD10 (5'-UGAAGCAGUGCAAGUACUA-3'), and human mitofilin (5'-AAUUGCUGGAGCUG GCCUU -3') and human YME1L (5'-UGAAGCAGUGCAAGUACUA-3'), human OPA1 (5'-CUG GAA AGA CUA GUG UGU U-3') were obtained from GE Dhamacon (Lafayette, CO, USA). Lentivirus construct expressing CHCHD10 shRNA was obtained from Abmgood (Richmond, BC, Canada). The generation of lentivirus has previously been described (8).

DNA/siRNA transfections and lentivirus transductions

DNA plasmids were transiently transfected in HEK293T, NIH3T3, Hela cells using fugene HD (Promega, Madison, WI, USA) and Opti-MEM I (Invitrogen, Carlsbad, CA, USA) according to the manufacturer's instructions. The lipofectamine 2000 (Invitrogen, CA, USA) and Opti-MEM I were used for siRNA transfections, and cells were transfected with siRNA twice every 24h. After four to six hours transfections, the medium was replaced with new complete medium. Generally, cells were incubated 24–48h for plasmid transfections and 72h for siRNA transfections prior to harvest. For lentivirus transduction in primary neurons, cells were transduced and incubated for 5d.

Antibodies and reagents

Anti-Mic23/Mic26 (2F1) (Cat#: NBP1-28870) primary antibody was obtained from Novus Biologicals (Centennial, CO, USA). Anti-YME1L1 (Cat#: 11510-1-AP) and anti-Mic19 (Cat#: 25625-1-AP) primary antibodies were obtained from Proteintech Group (Rosemont, IL, USA). Anti-M2 (Cat#: F3165) and β-actin (Cat#: A2228) monoclonal antibody were obtained from Sigma-Aldrich (St. Louis, MO, USA). Anti-myc (Cat#: 2276), OPA1 (Cat#: 67589), Tom20 (Cat#: 42406), TDP-43 (G400, Cat#: 3448) primary antibodies were purchased from Cell Signaling (Danvers, MA, USA). Anti-Complex II (Cat#: 459200) primary antibody was purchased from Invitrogen (Camarillo, CA, USA). Anti-TDP-43 antibody (Cat#: H00023435-M01) was purchased from Abnova (Walnut, CA, USA). Anti-CHCHD10 (Cat#: ab121196) primary antibody was obtained from Abcam (Cambridge, UK). Anti-mitofilin (Cat#: sc-390706) primary antibody were obtained from Santa Cruz (Dallas, TX, USA). BMH (bismaleimidohexane) crosslinker was purchased from Sigma-Aldrich (St. Louis, MO, USA).

SDS-PAGE, Blue Native gel electrophoresis

RIPA lysis buffer (50mM Tris pH 7.4, 150mM NaCl, 2mM ethlenediaminetetra acetic acid, 1% NP-40, 0.1% sodium dodecyl sulfate) was used lyse cells. Total protein concentrations were measured by a colorimetric detection assay (BCA Protein Assay, Pierce, USA). Equal protein amounts of protein lysates were separated by SDS-PAGE and transferred to nitrocellulose membranes (Bio-Rad, Hercules, CA, USA). For native gel immunoblotting, cells or tissues were lysed using NativePAGE Sample Prep Kit (ThermoFisher Scientific, MA, USA), which uses the mild detergent digitonin to retain native protein complexes. Equal protein amounts of protein lysates were separated by Blue Native gel (ThermoFisher Scientific, MA, USA) electrophoresis, and transferred to Immunobilon-P PVDF membranes (Millipore Corporation, Bedford, MA, USA).

Mito-dendra2 mitochondrial fusion assay

Mitochondrial fusion assays were performed by photoconversion and live cell imaging with the ZEISS LSM880 confocal microscope (ZEISS, Jena, Germany) in a caged humidified chamber at 37°C using Hibernate-A medium (Thermo Scientific, MA, USA). For photo-conversion of mito-dendra2 in live cells, a region of interest (ROI) was illuminated with the 405 nm line with 4% laser power for 40 seconds. The 488 nm laser line with 5% laser power and the 561 nm laser line with 8% laser power were used to excite mito-dendra2 in the

unconverted state and photo-converted state, respectively, and images were acquired for 250 iterations over a period of 20 minutes. The percentages of co-localization within the ROI from acquired images were measured by using COLOC2 plugin of Image J software (NIH, Bethesda, MD, USA) with identical threshold and adjustment of brightness/contrast.

Seahorse mitochondrial respiration assay

Prior to the day of mitochondrial respiration assay, the utility plate (Agilent, CA, USA) was incubated with sterile water at 37°C in a non-CO_2 incubator for overnight and water was replaced with Searhorse XF calibrant (Agilent, CA, USA) the next day for 1h. On the day of the assay, cells were washed with assay medium (DMEM base medium supplemented with 10 mM glucose, 1 mM pyruvate, 2 mM Glutamine, pH 7.4) and incubated with this assay medium at 37°C in a non-CO_2 incubator for 1h. Four baseline measurements of OCR were taken before sequential injection of mitochondrial inhibitors including oligomycin (1.5 M), FCCP (1.0 M), and Antimycin (0.5 M)/rotenone (0.5 M) from the XF Cell Mito Stress Test Kit (Agilent, CA, USA). The OCR measurement was performed using Seahorse XFe96 analyzer (Agilent, CA, USA). After the assays, plates were saved and subjected to protein measurement to confirm equal protein concentration of assayed cells.

Immunocytochemistry and *in situ* proximity ligation assay

For immunocytochemistry (ICC), cells were washed with PBS and fixed at room temperature for 15 minutes with 4% paraformaldehyde (PFA). Then cells were washed with PBS and incubated with blocking solution containing 0.2% Triton X-100, 3% normal goat serum for 1h, followed by overnight incubation at 4°C with related primary antibodies. Then cells were washed with PBST (phosphate buffered saline with Triton X-100) for three times followed by 1h incubation with Alexa-488 or Alexa-594 conjugated secondary IgG antibodies (Vector Laboratories, Burlingame, CA). Slides were then washed three times with PBST and mounted with fluorochrome mounting solution (Vector Laboratories) as previously described (39).

For *in situ* proximity ligation assay (PLA), two antibodies (raised in different species) for corresponding proteins are applied, after which a pair of oligonucleotide-labeled secondary antibodies bind to primary antibodies. If in close proximity to each other (~40 angstroms) (40), connector oligos join the PLA probes and are ligated to form circular DNA that are amplified by DNA polymerase. This allows up to 1000-fold amplification, and complementary detection oligos coupled to a fluorochrome are hybridized to detect the PLA signal. For Duolink *in situ* PLA, fixed cells or tissues were permeabilized and blocked blocking solution containing 0.2% Triton X-100, 3% normal goat serum for 1h followed by PBS washing. Then they were incubated with two interested primary antibodies diluted in blocking solution containing 0.2% Triton X-100, 3% normal goat serum for overnight at 4°C. They were washed with PBS for seven times. Then cells or tissues were incubated with oligonucleotide-labelled PLA probes (PLUS/MINUS) (Sigma Aldrich, St Louis, MO, USA) diluted in blocking solution for 30 min at 37°C. They were washed with Duolink wash solution A (Sigma Aldrich, St Louis, MO, USA) and the ligation and amplifications were performed as instructed in the manufacturer's protocol. Then the cells/tissues were

immunostained or DAPI-stained (Invitrogen) and mounted on slides using nail polish as previously described (37).

All images were captured with the Olympus FV10i confocal microscope using 60x objective lens (Tokyo, Japan) or ZEISS LSM880 confocal microscope using 40x objective lens, and the immunoreactivities were quantified from hippocampus region using the Image J software (National Institutes of Health, Bethesda, MD, USA). In ICC and PLA experiments, all comparison images were acquired with identical laser intensity, exposure time, and filter. Regions of interest were chosen randomly, and investigators were blinded to genotypes of mice and experimental conditions during image acquisition and quantification. Adjustments to the brightness/contrast were applied equally to all comparison images.

Statistical analysis

All graphs were analyzed and made using GraphPad Prism 6.0 software (GraphPad Software, San Diego, CA, USA) using student's *t*-test, 1-way analysis of variance (ANOVA) followed by Tukey post hoc test, or 2-way ANOVA followed by Sidak post hoc test. Differences were deemed significant when $P<0.05$. Quantified results are expressed as mean ± S.E.M (error bars).

Results

Transgenic mice expressing human CHCHD10 variants in the CNS

Two recent studies reported the generation and characterization of the CHCHD10^{S59L} knock-in mouse model, in which the mutant allele is expressed under control of the endogenous mouse *CHCHD10* promoter (41, 42). These mice were reported to develop mitochondrial cardiomyopathy and myopathy prior to onset of spinal motor neuron disease; however, brain regions were relatively unaffected (41, 42). To study the role of wild type CHCHD10 and FTD/ALS-linked CHCHD10 mutations (S59L & R15L) in the central nervous system (CNS), we sought to develop transgenic mouse models with enriched human CHCHD10 expression in neurons of the brain and spinal cord, which are primarily affected in FTLD and ALS, respectively. Hence, we generated transgenic Flag-CHCHD10 variants (D10-WT, R15L, & S59L) driven by the mouse *PrP* promoter (Fig. 1a), akin to those previously described for APP/PS1 (34), PS19 tauP301S (35), and -synuclein A53T (36) transgenic models. The genotypes of transgenic mice were identified by PCR using genomic DNA (Supplemental Fig. S1a) and by Western blotting (Supplemental Fig. S1b–d; Fig. 1c). From transgenic strains best matched for Flag-CHCHD10 levels (Fig. 1c), real-time quantitative RT-PCR using 2 primer sets common to mouse and human CHCHD10 mRNA sequences showed that human WT, R15L, and S59L CHCHD10 transcripts were similarly expressed at 2.5-2.8-fold higher than the endogenous CHCHD10 transcript in brain (Fig. 1b). Western blotting for CHCHD10 proteins showed that human CHCHD10 variants were widely expressed in all CNS regions examined (Supplemental Fig. S1f–h), similar to endogenous CHCHD10 (Supplemental Fig. S1e). However, the Flag-R15L but not Flag-S59L mutant protein was expressed at ~50% of Flag-CHCHD10-WT levels (Fig. 1c), which may be attributed to the instability of the R15L mutant as previously reported (43, 44).

FTD/ALS-linked CHCHD10 mutations disrupt OPA1-mitofilin complexes in transfected cells and *in vivo*

The FTD/ALS-linked CHCHD10 S59L mutation disrupts mitochondrial cristae structure and exhibits reduced binding to mitofilin (24, 31, 32). In addition to other MICOS components, mitofilin also interacts with OPA1, an inner membrane protein best known for its role in mitochondrial fusion (18) and regulation of cristae integrity (22, 23). Hence, we looked for evidence of CHCHD10-mediated regulation of both OPA1 and mitofilin in 10-month old CHCHD10 transgenic mouse variants (D10-WT, R15L, & S59L). We observed no significant changes in mitofilin between any of the transgenic groups (Fig. 1d,e). The 2 major precleaved L-OPA1 bands (~90-95 kDa) were also unchanged by D10-WT or CHCHD10 mutations (R15L & S59L) compared to WT mice (Fig. 1d,f). Interestingly, higher exposure of the blot revealed that the ~75–80 kDa cleaved S-OPA1 fragments were significantly increased in S59L transgenic mice compared to WT, D10-WT, or R15L transgenic mice (Fig. 1d,g). Overall levels of Drp1 and Mfn2, mitochondrial outer membrane fission and fusion associated proteins, respectively, were not significantly altered by CHCHD10 variants in brain (Fig. 1d; Supplemental Fig. S2a,b). Although R15L and S59L transgenic mice exhibited a minor trend toward reduced endogenous CHCHD2 levels, this difference was not found to be significant (Fig. 1d; Supplemental Fig. 2c).

As OPA1 is known to form a complex with mitofilin (22, 23), we next assessed the OPA1-mitofilin complex using Duolink *in situ* proximity ligation assay (PLA) in transfected cells and CHCHD10 transgenic mouse brains (see Supplemental methods). Using PLA and two antibodies directed against OPA1 and mitofilin, we detected endogenous OPA1-mitofilin complexes as PLA puncta (Fig. 1h,j). Exclusion of 1 primary antibody or 1 secondary probe yielded no detectable PLA signal, indicating the specificity of the assay (Supplemental Fig. S2d). Surprisingly, WT CHCHD10 transfection in NIH3T3 cells increased the endogenous OPA1-mitofilin complex by nearly 2-fold, whereas R15L or S59L mutants significantly reduced this complex by up to 65% compared to vector control (Fig. 1h,i). Similar changes in endogenous OPA1-mitofilin complex was also observed in CHCHD10 transgenic brains, in which WT CHCHD10 significantly increased the OPA1-mitofilin complex by 1.75-fold compared to nontransgenic littermates, whereas R15L and S59L mutations dramatically reduced OPA1-mitofilin complex by 50% and 70%, respectively, in the hippocampus CA3 region (Fig. 1j,k). Nearly identical results were observed in the frontal cortex of CHCHD10 transgenic variants (Supplemental Fig. S2e,f).

FTD/ALS-linked CHCHD10 mutations exhibit reduced binding to OPA1 and mitofilin and disrupt high molecular weight native CHCHD10, mitofilin, and OPA1 *in vivo*

To better understand the mechanistic basis of CHCHD10 mutations in destabilization of the OPA1-mitofilin complex, we tested the extent to which CHCHD10 variants can associate with endogenous OPA1 and mitofilin *in situ*. Hence, we co-transfected NIH3T3 cells with WT CHCHD10 or CHCHD10 mutations (R15L & S59L) together with GFP in a 3:1 ratio and performed PLA to detect OPA1-CHCHD10 and mitofilin-CHCHD10 complexes. Quantification of PLA puncta normalized to GFP intensity showed that both R15L and S59L mutants exhibit significantly reduced binding to both OPA1 and mitofilin (Fig. 2a–d). Interestingly, the extent to which the mutations reduce binding to OPA1 and mitofilin were

distinctly different, with the S59L mutations exhibiting a more severe loss of OPA1 binding and the R15L mutation exhibiting a more severe loss of mitofilin binding (Fig. 2a–d). Co-immunoprecipitation (co-IP) experiments likewise showed that wild type CHCHD10 binds to both mitofilin and OPA1, whereas CHCHD10 mutations (R15L & S59L) exhibit markedly reduced binding compared to WT CHCHD10 (Supplemental Fig. S2g). We also confirmed that endogenous CHCHD10 and mitofilin co-immunoprecipitates with endogenous OPA1 (Supplemental Fig. S2h).

To gain further insights to the nature of mitofilin, OPA1, and CHCHD10 complexes, we assessed CHCHD10 transgenic mouse brains by native blue gel electrophoresis after digitonin extraction to maintain native protein complexes (45). Surprisingly, D10-WT transgenic extracts showed a dramatic 2.5-fold increase in 480-720 kDa native OPA1 bands compared to WT extracts, whereas R15L and S59L mutations largely collapsed the 480-720 kDa native OPA1 bands to under 300 kDa (Fig. 2e,f), indicating that these mutations severely disrupt native OPA1 protein complexes. The native ~720 kDa mitofilin complex was modestly but significantly reduced by R15L and S59L mutations compared to WT and D10-WT transgenic mice (Fig. 2e,g). Assessment of native CHCHD10 showed that WT human Flag-CHCHD10 incorporates into the ~720 kDa, ~480 kDa, and ~300 kDa bands, whereas the R15L and S59L mutations exhibit a different banding pattern (Fig. 2e). Quantification of the bands normalized to the expression level of transgenic Flag-CHCHD10 variants showed that R15L and S59L mutations exhibit severely diminished capacity to incorporate into 480-720 kDa bands compared to CHCHD10-WT (Fig. 2h). Endogenous mouse CHCHD10 was largely seen in the ~720 kDa band (Fig. 2e).

FTD/ALS-linked CHCHD10 mutations impair mitochondrial fusion and respiration

As OPA1 and the OPA1-mitofilin complex play critical roles in mitochondrial inner membrane fusion (18), we next assessed whether CHCHD10 variants alter mitochondrial fusion. Hence, we performed mitochondrial fusion assays using the mito-dendra2 reporter, in which dendra2 is targeted to mitochondria (38). Dendra2 is a photoconvertible fluorescent protein that normally possesses excitation-emission maxima at 490/507nm (like GFP). Upon photoconversion at 405nm, the excitation/emission spectra permanently shift to 553/573nm, thereby converting from green to red fluorescent state. This allows the tracking of the photoconverted mito-dendra2 protein (red) in a specific subcellular region of interest (ROI) and its subsequent fusion with unconverted mito-dendra2 (green), thereby yielding a yellow/orange signals upon fusion (38). To confirm the utility of the assay, we first co-transfected control siRNA or OPA1 siRNA together with mito-dendra2. Upon photoconversion of a small ROI (white boxes) for 40 seconds and live cell imaging over 20 minutes, we observed progressive conversion of red signals to yellow (red+green colocalization) over 20 minutes, indicative of mitochondrial fusion (Fig. 3a,b). In OPA1 siRNA transfected cells, the photoconverted ROI remained largely red and orange over the 20-minute period (Fig. 3a,b), confirming the significant loss of mitochondrial fusion by OPA1 siRNA. For assessment of CHCHD10 variants, we transfected CHCHD10 variants and mito-dendra2 at a ratio of 2:1 to ensure that mito-dendra2 expressing cells also express CHCHD10. Photoconversion and live cell imaging over 20 minutes showed that both R15L and S59L transfected cells exhibit significantly slower mitochondrial fusion compared to vector control and WT CHCHD10,

although the S59L mutation showed a more severe phenotype (Fig. 3c,d). Wild type CHCHD10 transfected cells exhibited similar mitochondrial fusion as vector control transfected cells (Fig. 3c,d).

As both mitofilin and OPA1 complexes are critical for the regulation of mitochondrial respiration (16, 17, 46, 47), we performed the mitochondria stress test using Seahorse technology, which measures mitochondrial oxygen consumption rate in response to sequential treatments of oligomycin (Complex V ATP synthase inhibitor), FCCP (mitochondrial decoupler), and rotenone/antimycin (Complex I & III inhibitors). Both R15L and S59L mutations significantly reduced basal respiration, maximal respiration, and respiration attributed to ATP production compared to WT CHCHD10 (Fig. 3e–h). The S59L mutation generally exhibited a more severe phenotype than the R15L mutation, and WT CHCHD10 showed nonsignificant increases in all measures of respiration compared to vector control (Fig. 3e–h).

Knockdown of endogenous CHCHD10 destabilizes MICOS components and OPA1-mitofilin complex

Mitofilin *per se* is required to maintain the stability of other components of the MICOS complex (10). However, the functional role of endogenous CHCHD10 in MICOS complex is unknown. Given the reduction of CHCHD10 in brains of FTLD-TDP patients, we next assessed the effects of endogenous CHCHD10 knockdown. We transfected HEK293T cells with CHCHD10 siRNA, isolated mitochondria, and looked for several key MICOS subunits (mitofilin, mic23/mic26, and mic19) by Western blotting. Knockdown of endogenous CHCHD10 significantly reduced all 3 MICOS components, although the reduction in mitofilin was the least severe (Fig. 4a,b). YME1L is an inner membrane AAA protease known to degrade various proteins at the inner membrane and intermembrane space (IMS) (48). Knockdown of YME1L together with CHCHD10 prevented CHCHD10 knockdown-induced reduction in mitofilin, mic23/mic26, and mic19 (Supplemental Fig. S3a), indicating that these proteins are degraded by YME1L upon transient loss of CHCHD10. To assess native mitofilin complexes, we next isolated mitochondria, lysed mitochondria with digitonin, and subjected proteins to blue native gel electrophoresis. In HEK293T cells, we observed 2 prominent bands migrating at ~720 kDa and 480 kDa positive for mitofilin. Knockdown of CHCHD10 significantly reduced both mitofilin bands by >50% (Fig. 4c,d), confirming that the loss of CHCHD10 disrupts native mitofilin complexes.

As done for CHCHD10 overexpression, we looked for evidence of CHCHD10-mediated regulation of OPA1. Knockdown of endogenous CHCHD10 did not produce salient changes in L-OPA1 or the cleaved S-OPA1 (Supplemental Fig. S3b–d). However, assessment by blue native gels showed the presence of a prominent ~720 kDa native OPA1 band, which was significantly reduced by ~50% upon silencing CHCHD10 (Fig. 4e,f). We next conducted co-immunoprecipitation (co-IP) experiments to assess OPA1-mitofilin interaction. As predicted, knockdown of CHCHD10 saliently reduced mitofilin in the myc-OPA1 immune complex even the presence of YME1L silencing (Fig. 4g). The specificity of the myc-OPA1/mitofilin complex was confirmed by FCCP treatment, which is known to disrupt OPA1 complexes and induce OPA1 cleavage (Supplemental Fig. S3e). Indeed, the loss of the OPA1-mitofilin

complex by CHCHD10 silencing was as effective as FCCP treatment even with YME1L knockdown (Supplemental Fig. S3e). Finally, we confirmed a ~70% reduction of the endogenous OPA1-mitofilin complex in NIH3T3 cells transduced with CHCHD10-shRNA-GFP lentivirus as assed by *in situ* PLA (Fig. 4h,i).

TDP-43 reduces CHCHD10 and disrupts native CHCHD10, OPA1, and mitofilin complexes in brains of human FTLD-TDP and TDP-43 transgenic mice

Multiple studies have shown that the accumulation of TDP-43 in mitochondria of neurons induces mitochondrial dysfunction and synaptic damage (8–10). These observations together with the current finding that FTD/ALS-linked CHCHD10 mutations disrupt mitofilin and OPA1 complexes prompted us to examine whether CHCHD10 and mitofilin levels are altered in human TDP-43 proteinopathy. In RIPA extracts from the frontal gyrus of FTLD-TDP patients and age-matched nondemented controls, we observed a significant ~30% reduction in CHCHD10 levels (Fig. 5a,b) in FTLD-TDP (n=10) compared to nondemented controls (n=13) without significant changes in mitofilin levels (Fig. 5a,c). Cleaved S-OPA1 bands migrating ~75-85 kDa were significantly increased by ~70% in FTLD-TDP compared to nondemented controls (Fig. 5a,d). Although difficult to detect from human postmortem tissues, assessment and quantification of native CHCHD10, mitofilin, and OPA1 by digitonin extraction in blue native gels showed that all three proteins were significantly reduced in the ~720 kDa band in FTLD-TDP compared to nondemented control (Supplemental Fig. S4a–d), suggesting that TDP-43 accumulation might underlie this disruption. Hence, we assessed TAR4 mice, which express WT human TDP-43 driven by the Thy-1 promoter and exhibits prominent TDP-43 pathology (33). Compared to WT littermates, 18-month old TAR4 mouse brains exhibited a significant 60% reduction in CHCHD10 (Fig. 5e,f) without significantly altering mitofilin, L-OPA1, or cleaved S-OPA1 in the RIPA extracts (Fig. 5e,g,h). Digitonin-extracted ~720 kDa native CHCHD10 and mitofilin bands were also significantly reduced in TAR4 mouse brains compared to littermate controls (Supplemental Fig. S4e–g). *In situ* PLA experiments to detect OPA1-mitofilin complexes indeed showed a significant ~40% reduction in OPA1-mitofilin PLA puncta in TAR4 mouse brains compared to wild type littermate brains (Fig. 5i,j), demonstrating an identical biochemical signature as those seen in mutant CHCHD10 (R15L & S59L) transgenic mouse brains. Likewise, overexpression of TDP-43 in HEK293T cells also showed a dramatic disruption of the native ~720 kDa mitofilin band from the mitochondrial fraction (Supplemental Fig. S4h,i).

We previously showed that TDP-43 physically interacts with CHCHD10 (8). To gain mechanistic insights to TDP-43-induced disruption of mitofilin and OPA1 complexes, we assessed if TDP-43 can form stable complexes with mitofilin or OPA1. Hence, we performed biochemical co-IP experiments after transfection of HEK293T cells with or without TDP-43-myc. However, myc immune complexes did not contain specific bands corresponding to either mitofilin or OPA1 even through TDP-43-myc was robustly pulled down (Supplemental Fig. S4j), suggesting that TDP-43 does not form a stable complex with mitofilin or OPA1. Under identical biochemical conditions, Flag-CHCHD10 formed a complex with both endogenous mitofilin and OPA1 (Supplemental Fig. S4k). Upon transfection of TDP-43-myc, we detected formation of the TDP-43/CHCHD10 complex,

which coincided with abolition of the CHCHD10-mitofilin complex and markedly reduced CHCHD10-OPA1 complex (Supplemental Fig. S4k). These findings therefore suggest that, in addition to reducing endogenous CHCHD10, the binding of TDP-43 to CHCHD10 interferes with the ability of CHCHD10 to form complexes with mitofilin and OPA1.

TDP-43 recapitulates mitochondrial abnormalities associated with CHCHD10 mutations and are rescued by wild type CHCHD10

As TDP-43 interfered with the ability of CHCHD10 to form complexes with OPA1 and mitofilin and reduced endogenous CHCHD10, we hypothesized that TDP-43-induced mitochondrial abnormalities are at least in part through CHCHD10. If so, then TDP-43 should recapitulate mitochondrial phenotypes associated with FTD/ALS-linked CHCHD10 mutations and increasing wild type CHCHD10 expression should at least partially rescue TDP-43-induced mitochondrial phenotypes. Hence, we first performed *in situ* PLA experiments in NIH3T3 cells to detect the OPA1-mitofilin complex upon transfection of GFP or GFP-TDP-43 with/without OPA1-myc and/or Flag-CHCHD10. We detected the endogenous OPA1-mitofilin complex, which more than doubled with transfection of OPA1-myc (Fig. 6a,b). Transfection of OPA1-myc with CHCHD10 further significantly increased OPA1-mitofilin complexes by ~55% (Fig. 6a,b), in agreement with our CHCHD10 knockdown results (Fig. 4h,i). Transfection of GFP-TDP-43 with OPA1-myc drastically reduced the OPA1-mitofilin complex by ~70% compared to OPA1-myc alone (Fig. 6a,b), thereby recapitulating the effects of CHCHD10 mutations and knockdown. Expression of CHCHD10 with GFP-TDP-43 + OPA1-myc, in contrast, fully restored the OPA1-mitofilin complex to levels seen with OPA1-myc transfection alone (Fig. 6a,b). Similarly, primary cortical neurons derived from TAR4 mice or HEK293T cells transfected with TDP-43 exhibited significant disruption of the native mitofilin complex, which was largely restored in cortical neurons derived from TAR4;CHCHD10 double transgenic littermates or HEK293T cells co-transfected with CHCHD10 (Supplemental Fig. S5a–c).

To determine whether TDP-43 produces functional changes associated with disruption of OPA1-mitofilin complexes and whether wild type CHCHD10 can rescue such changes, we transfected NIH3T3 cells with TDP-43+vector or TDP-43+CHCHD10 together with mito-dendra2 at a ratio of 1 mito-dendra2 to 2 TDP-43, vector, or CHCHD10. TDP-43 expression resulted in significantly slower mitochondrial fusion compared to vector alone over a 20-minute period after photoconversion (Fig. 6c,d). However, co-expression of TDP-43 with CHCHD10 restored the rate of mitochondrial fusion to vector control levels (Fig. 6c,d), consistent with the rescue of TDP-43-induced disruption of the OPA1-mitofilin complex by CHCHD10. Likewise, assessment of mitochondrial respiration showed a dramatic reduction in mitochondrial respiration by TDP-43, which was significantly restored to near control levels by CHCHD10 overexpression (Fig. 6e–g).

Discussion

FTLD-TDP and ALS patients exhibit severe mitochondrial abnormalities (3–5), which are closely associated with TDP-43 pathology (6, 7). In this study, we made a series of novel observations regarding the interplay between CHCHD10 and TDP-43 utilizing transfected

cells, CHCHD10 transgenic mice, TDP-43 transgenic (TAR4) mice, and FTLD-TDP brains. The CHCHD10 transgenic mouse variants (WT, R15L, & S59L) described in this study represent the first mouse models of human CHCHD10 variant expression enriched in the CNS. Using these transgenic models, we showed that FTD/ALS-linked CHCHD10 mutations disrupt the OPA1-mitofilin complex in brain to impair mitochondrial fusion and respiration, whereas wild type CHCHD10 promotes the OPA1-mitofilin complex. Such changes by FTD/ALS-linked CHCHD10 mutations were recapitulated in brains of FTLD-TDP patients as well as cellular and animal models of TDP-43, as seen by the loss of the OPA1-complex as well as impaired mitochondrial fusion and respiration. Importantly, these TDP-43-induced mitochondrial abnormalities were rescued by expression of wild type CHCHD10, supporting the notion that CHCHD10 mutations and TDP-43 produce mitochondrial dysfunction through convergent mechanisms and that the loss of endogenous CHCHD10 expression or activity at least in part drives TDP-43-induced deficits in mitochondrial fusion and respiration through disruption of the OPA1-mitofilin complex.

Our findings showed for the first time that CHCHD10 mutations (R15L & S59L) strikingly disrupt the OPA1-mitofilin interaction, with S59L being more severe than R15L, whereas WT CHCHD10 robustly increases this interaction, suggesting that CHCHD10 functions to bridge the interaction between OPA1 and mitofilin. Interestingly, the interaction between CHCHD10 and OPA1 was more severely deficient with the S59L mutation compared to the R15L mutation, whereas the interaction between CHCHD10 and mitofilin was more severely reduced by the R15L mutation, suggesting that the mechanism of OPA1-mitofilin complex disruption may be subtly different between the 2 mutations. This may be partially explained by the observation that the S59L but not R15L mutation significantly increased the cleaved S-OPA1 isoforms compared to WT CHCHD10 transgenic brains. As the cleaved S-OPA1 fragment generally favors mitochondrial fission versus fusion (46, 49), such increase in S-OPA1 likely accounts for the more severe mitochondrial fusogenic phenotype associated with the S59L mutation. Nevertheless, our biochemical and imaging studies showed that OPA1 complex assembly and OPA1-mitofilin interaction were disrupted by both S59L and R15L mutations, indicating that the increase in S-OPA1 is an added feature of the S59L mutation accounting for more severe mitochondrial phenotypes. Like mitofilin and L-OPA1, we observed no detectable differences in the overall levels of Mfn2, Drp1, or CHCHD2 proteins. However, we cannot rule out the possibility that different complexes of these proteins are altered by CHCHD10 mutations, particularly CHCHD2, which has been reported to form a complex with CHCHD10 (44, 50–52). Interestingly, a recent study using a *Drosophila* model reported that the wild type version of *Drosophila* CHCHD2 increases OPA1 levels, while CHCHD2 mutations decrease OPA1 through as yet unknown mechanism (53).

Disruption of native high molecular weight (HMW) mitofilin bands by R15L and S59L mutations closely mirrored the disruption of the native HMW CHCHD10 bands by the same mutations, suggesting that the loss of CHCHD10 incorporation into HMW native CHCHD10 bands destabilizes the native mitofilin complex in brain, a complex linked to mitochondrial cristae integrity (13). It is also likely that changes in the OPA1-mitofilin complex contribute to the observed alterations in mitochondrial respiration seen by CHCHD10 variants (17, 18, 22). It is also notable that while WT CHCHD10 dramatically

increased the HMW native OPA1 complex and OPA1-mitofilin interaction, WT CHCHD10 failed to increase the HMW native mitofilin complex, consistent with mitofilin *per se* as a rate limiting factor in the assembly of MICOS (13). This also suggests that the native HMW mitofilin complex may be largely distinct from and epistatic to the native HMW OPA1 complex with only partial overlap, such as CHCHD10 (23). Aside from the ~720 kDa MICOS complex containing at least mitofilin, CHCHD10, Mic19, Mic25, Mic27, Mic23, Mic10, and Mic12 (54), we also observed ~480 kDa and ~300 kDa native complexes from mouse brains. The ~480 kDa complex containing mitofilin and CHCHD10 is reminiscent of the ~450-600 kDa MICOS Centerpiece complex thought to contain at least mitofilin, Mic19, and Mic25 (54–56). While the ~300 kDa complex remains to be fully defined, native OPA1 and CHCHD10 but not mitofilin were detected at this molecular weight, especially in R15L and S59L transgenic brains.

Our novel finding that knockdown of endogenous CHCHD10 destabilizes MICOS components mitofilin, Mic23, and Mic19 argues that endogenous CHCHD10 has an essential role in MICOS assembly through the binding and stabilization of the complex, the loss of which leads to YME1L-mediated degradation of its subunits. Although constitutive *CHCHD10*$^{-/-}$ cells display only subtle mitochondrial respiration deficits (30), this may be due to the upregulation of *CHCHD2*, a partially redundant *CHCHD10* homolog that forms a complex with CHCHD10 (8, 50, 51) and is known to be upregulated in response to mitochondrial stress (44, 57). In our experimental setting, we used transient knockdown of CHCHD10, which does not result in increased CHCHD2 (8). While RNAi-mediated CHCHD10 knockdown failed to alter OPA1 levels, CHCHD10 knockdown drastically reduced the native OPA1 complex and OPA1-mitofilin interaction. Hence, we interpret these results to indicate that endogenous CHCHD10 also constitutes a key component mediating the stabilization of OPA1-mitofilin complex, likely by bridging this interaction. In this context, the observation that R15L and S59L mutations disrupt the OPA1-mitofilin interaction suggests that these mutations may exert a dominant negative activity on this complex, by binding to mitofilin and/or OPA1 but failing to stabilize the cross-interaction.

The observation that the CHCHD10 protein is significantly reduced in brains of FTLD-TDP patients indicates that phenotypes associated with CHCHD10 reduction may be pathogenically relevant to FTLD-TDP. Indeed, disease-linked CHCHD10 mutations R15L and G66V mutations exhibit reduced CHCHD10 levels and increased turnover, indicative of partial haploinsufficiency (43, 44). FTLD-TDP brains and TDP-43 transgenic mice not only exhibited reduced CHCHD10 protein but also disruptions in native CHCHD10, mitofilin, and OPA1 assemblies. It is notable that TDP-43-induced loss of the native CHCHD10 complex was more severe than the loss of either native mitofilin or OPA1 complexes, suggesting that the loss of CHCHD10 from native HMW assemblies may trigger the loss of OPA1 and/or mitofilin from these complexes in brain. Indeed, co-IP and PLA experiments revealed that TDP-43 binds to CHCHD10 and interferes with the ability of CHCHD10 to form complexes with OPA1 and mitofilin, thereby recapitulating the effects of CHCHD10 mutations. While human FTLD-TDP brains exhibited a significant increase in cleaved S-OPA1 isoforms, TDP-43 transgenic mice only showed a mild but nonsignificant increase in S-OPA1. This suggests that the OPA1 phenotype is more severe in human FTLD-TDP

compared to TDP-43 transgenic mice and that disruption of the OPA1-mitofilin complex is an earlier and separable TDP-43-related phenotype versus S-OPA1 generation.

Under pathological conditions, TDP-43 mislocalizes from the nucleus to cytoplasm and is associated with the ER, RNA granules, mitochondria-associated membranes (MAMs), and mitochondria (8, 10, 58–61). Within mitochondria, TDP-43 reduces mitochondrial length by promoting mitochondrial fission (11). Mitochondrial fission and fusion are in dynamic balance, in which loss of fission (i.e. Drp1, Fis1) favors fusion, and loss of fusion (Mfn1/2, OPA1) favors fission (62). While fragmented mitochondria are associated with reduced membrane potential and health, fusion of mitochondria (elongated) increases mtDNA and protein components needed to rejuvenate mitochondria (62, 63). TDP-43 experimental models demonstrate tipping of the balance toward increased fission, as TDP-43 induces the loss of Mfn1 as well as increased Drp1 and Fis (7, 64, 65). Moreover, TDP-43 expression is associated with disruption of mitochondrial cristae structure as well as reduced mitochondrial respiration (6, 66). In this context, the observation that TDP-43 recapitulates the mitochondrial phenotypes (OPA1-mitofilin interaction, fusion, & respiration) associated with CHCHD10 mutations is intriguing. But more importantly, the finding that these TDP-43-induced mitochondrial defects are largely rescued by wild type CHCHD10 indicates that TDP-43 drives mitochondrial impairments in large part through CHCHD10 deregulation. As CHCHD10 fully rescued the defects in OPA1-mitofilin interaction and mitochondrial fusion induced by TDP-43 but partially rescued TDP-43-induced impairments in mitochondrial respiration, factors other than CHCHD10-depenent OPA1-mitofilin complex also contribute to overall mitochondrial defects associated TDP-43 (6, 65). As examples, neither Drp1 nor Mfn2 were altered in mutant CHCHD10 transgenic mice, whereas Drp1, Fis1, and Mfn1 were found to be altered by TDP-43 (7, 64, 65). Collectively, these results support the notion that destabilization of the native CHCHD10 complex and OPA1-mitofilin interaction significantly contribute to mitochondrial abnormalities in FTLD-TDP brains and that increasing CHCHD10 expression could be beneficial to mitigating mitochondrial dysfunction in FTLD-TDP.

Supplementary Material

Refer to Web version on PubMed Central for supplementary material.

Acknowledgements

We thank Dr. Alexander M. van der Bliek (University of California, Los Angeles, CA) for providing OPA1-myc construct, Drs. Allan Levey and Gearing (Emory University) for providing postmortem human brain tissues, Dr. David Borchelt (University of Florida) for providing the MoPrP.Xho transgenic construct, and Dr. Don Cleveland (University of California, San Diego) for providing the tet-inducible Myc-TDP-43 cell line. This work was supported in part by grants from the NIH (1RF1AG053060-01A1, D.E.K; 5R01NS073899, D.E.K), VA (1 I01 BX002478-01A1, D.E.K.), and Florida department of Health (8AZ29, D.E.K & J.A.W.).

Nonstandard Abbreviations

CHCHD10	Coiled-coil-helix-coiled-coil-helix domain containing 10
CMT2	Charcot-Marie-Tooth disease type 2

FTD–ALS	frontotemporal dementia–amyotrophic lateral sclerosis
FTLD-TDP	frontotemporal lobar degeneration with TDP-43 pathology
HMW	high molecular weight
ICC	immunocytochemistry
IHC	immunohistochemistry
MAMs	mitochondria-associated membranes
MICOS	mitochondria contact site and cristae organization system
OPA1	Optic atrophy 1
PFA	paraformaldehyde
PLA	proximity ligation assays
P/S	penicillin/streptomycin
RIPA	radioimmunoprecipitation assay buffer
ROI	region of interest
TDP-43	Transactive response DNA binding protein 43 kDa
WT	wild type

References

1. Lomen-Hoerth C, Anderson T, and Miller B (2002) The overlap of amyotrophic lateral sclerosis and frontotemporal dementia. Neurology 59, 1077–1079 [PubMed: 12370467]
2. Feneberg E, Gray E, Ansorge O, Talbot K, and Turner MR (2018) Towards a TDP-43-Based Biomarker for ALS and FTLD. Mol Neurobiol 55, 7789–7801 [PubMed: 29460270]
3. Muyderman H, and Chen T (2014) Mitochondrial dysfunction in amyotrophic lateral sclerosis - a valid pharmacological target? Br J Pharmacol 171, 2191–2205 [PubMed: 24148000]
4. Smith EF, Shaw PJ, and De Vos KJ (2017) The role of mitochondria in amyotrophic lateral sclerosis. Neurosci Lett
5. Borthwick GM, Johnson MA, Ince PG, Shaw PJ, and Turnbull DM (1999) Mitochondrial enzyme activity in amyotrophic lateral sclerosis: implications for the role of mitochondria in neuronal cell death. Ann Neurol 46, 787–790 [PubMed: 10553999]
6. Wang P, Deng J, Dong J, Liu J, Bigio EH, Mesulam M, Wang T, Sun L, Wang L, Lee AY, McGee WA, Chen X, Fushimi K, Zhu L, and Wu JY (2019) TDP-43 induces mitochondrial damage and activates the mitochondrial unfolded protein response. PLoS Genet 15, e1007947 [PubMed: 31100073]
7. Xu YF, Gendron TF, Zhang YJ, Lin WL, D'Alton S, Sheng H, Casey MC, Tong J, Knight J, Yu X, Rademakers R, Boylan K, Hutton M, McGowan E, Dickson DW, Lewis J, and Petrucelli L (2010) Wild-type human TDP-43 expression causes TDP-43 phosphorylation, mitochondrial aggregation, motor deficits, and early mortality in transgenic mice. J Neurosci 30, 10851–10859 [PubMed: 20702714]
8. Woo JA, Liu T, Trotter C, Fang CC, De Narvaez E, LePochat P, Maslar D, Bukhari A, Zhao X, Deonarine A, Westerheide SD, and Kang DE (2017) Loss of function CHCHD10 mutations in

cytoplasmic TDP-43 accumulation and synaptic integrity. Nat Commun 8, 15558 [PubMed: 28585542]

9. Jiang TC, Handley E, Brizuela M, Dawkins E, Lewis KEA, Clark RM, Dickson TC, and Blizzard CA (2019) Amyotrophic lateral sclerosis mutant TDP-43 may cause synaptic dysfunction through altered dendritic spine function. Dis Model Mech 12
10. Wang W, Wang L, Lu J, Siedlak SL, Fujioka H, Liang J, Jiang S, Ma X, Jiang Z, da Rocha EL, Sheng M, Choi H, Lerou PH, Li H, and Wang X (2016) The inhibition of TDP-43 mitochondrial localization blocks its neuronal toxicity. Nat Med 22, 869–878 [PubMed: 27348499]
11. Wang W, Li L, Lin WL, Dickson DW, Petrucelli L, Zhang T, and Wang X (2013) The ALS disease-associated mutant TDP-43 impairs mitochondrial dynamics and function in motor neurons. Hum Mol Genet 22, 4706–4719 [PubMed: 23827948]
12. Rampelt H, Zerbes RM, van der Laan M, and Pfanner N (2017) Role of the mitochondrial contact site and cristae organizing system in membrane architecture and dynamics. Bba-Mol Cell Res 1864, 737–746
13. Li H, Ruan Y, Zhang K, Jian F, Hu C, Miao L, Gong L, Sun L, Zhang X, Chen S, Chen H, Liu D, and Song Z (2016) Mic60/Mitofilin determines MICOS assembly essential for mitochondrial dynamics and mtDNA nucleoid organization. Cell Death Differ 23, 380–392 [PubMed: 26250910]
14. Kaurov I, Vancova M, Schimanski B, Cadena LR, Heller J, Bily T, Potesil D, Eichenberger C, Bruce H, Oeljeklaus S, Warscheid B, Zdrahal Z, Schneider A, Lukes J, and Hashimi H (2018) The Diverged Trypanosome MICOS Complex as a Hub for Mitochondrial Cristae Shaping and Protein Import. Curr Biol 28, 3393-+ [PubMed: 30415698]
15. Callegari S, Muller T, Schulz C, Lenz C, Jans DC, Wissel M, Opazo F, Rizzoli SO, Jakobs S, Urlaub H, Rehling P, and Deckers M (2019) A MICOS-TIM22 Association Promotes Carrier Import into Human Mitochondria. J Mol Biol
16. Harner M, Korner C, Walther D, Mokranjac D, Kaesmacher J, Welsch U, Griffith J, Mann M, Reggiori F, and Neupert W (2011) The mitochondrial contact site complex, a determinant of mitochondrial architecture. EMBO J 30, 4356–4370 [PubMed: 22009199]
17. Friedman JR, Mourier A, Yamada J, McCaffery JM, and Nunnari J (2015) MICOS coordinates with respiratory complexes and lipids to establish mitochondrial inner membrane architecture. Elife 4
18. Cho B, Cho HM, Jo Y, Kim HD, Song M, Moon C, Kim H, Kim K, Sesaki H, Rhyu IJ, Kim H, and Sun W (2017) Constriction of the mitochondrial inner compartment is a priming event for mitochondrial division. Nat Commun 8, 15754 [PubMed: 28598422]
19. Malka F, Guillery O, Cifuentes-Diaz C, Guillou E, Belenguer P, Lombes A, and Rojo M (2005) Separate fusion of outer and inner mitochondrial membranes. EMBO Rep 6, 853–859 [PubMed: 16113651]
20. Song Z, Ghochani M, McCaffery JM, Frey TG, and Chan DC (2009) Mitofusins and OPA1 mediate sequential steps in mitochondrial membrane fusion. Mol Biol Cell 20, 3525–3532 [PubMed: 19477917]
21. Del Dotto V, Mishra P, Vidoni S, Fogazza M, Maresca A, Caporali L, McCaffery JM, Cappelletti M, Baruffini E, Lenaers G, Chan D, Rugolo M, Carelli V, and Zanna C (2017) OPA1 Isoforms in the Hierarchical Organization of Mitochondrial Functions. Cell reports 19, 2557–2571 [PubMed: 28636943]
22. Frezza C, Cipolat S, Martins de Brito O, Micaroni M, Beznoussenko GV, Rudka T, Bartoli D, Polishuck RS, Danial NN, De Strooper B, and Scorrano L (2006) OPA1 controls apoptotic cristae remodeling independently from mitochondrial fusion. Cell 126, 177–189 [PubMed: 16839885]
23. Glytsou C, Calvo E, Cogliati S, Mehrotra A, Anastasia I, Rigoni G, Raimondi A, Shintani N, Loureiro M, Vazquez J, Pellegrini L, Enriquez JA, Scorrano L, and Soriano ME (2016) Optic Atrophy 1 Is Epistatic to the Core MICOS Component MIC60 in Mitochondrial Cristae Shape Control. Cell Rep 17, 3024–3034 [PubMed: 27974214]
24. Bannwarth S, Ait-El-Mkadem S, Chaussenot A, Genin EC, Lacas-Gervais S, Fragaki K, Berg-Alonso L, Kageyama Y, Serre V, Moore DG, Verschueren A, Rouzier C, Le Ber I, Auge G, Cochaud C, Lespinasse F, N'Guyen K, de Septenville A, Brice A, Yu-Wai-Man P, Sesaki H, Pouget J, and Paquis-Flucklinger V (2014) A mitochondrial origin for frontotemporal dementia and

amyotrophic lateral sclerosis through CHCHD10 involvement. Brain 137, 2329–2345 [PubMed: 24934289]

25. Johnson JO, Glynn SM, Gibbs JR, Nalls MA, Sabatelli M, Restagno G, Drory VE, Chio A, Rogaeva E, and Traynor BJ (2014) Mutations in the CHCHD10 gene are a common cause of familial amyotrophic lateral sclerosis. Brain 137, e311 [PubMed: 25261972]
26. Muller K, Andersen PM, Hubers A, Marroquin N, Volk AE, Danzer KM, Meitinger T, Ludolph AC, Strom TM, and Weishaupt JH (2014) Two novel mutations in conserved codons indicate that CHCHD10 is a gene associated with motor neuron disease. Brain 137, e309 [PubMed: 25113787]
27. Zhang M, Xi Z, Zinman L, Bruni AC, Maletta RG, Curcio SA, Rainero I, Rubino E, Pinessi L, Nacmias B, Sorbi S, Galimberti D, Lang AE, Fox S, Surace EI, Ghani M, Guo J, Sato C, Moreno D, Liang Y, Keith J, Traynor BJ, St George-Hyslop P, and Rogaeva E (2015) Mutation analysis of CHCHD10 in different neurodegenerative diseases. Brain 138, e380 [PubMed: 25833818]
28. Penttila S, Jokela M, Bouquin H, Saukkonen AM, Toivanen J, and Udd B (2015) Late onset spinal motor neuronopathy is caused by mutation in CHCHD10. Ann Neurol 77, 163–172 [PubMed: 25428574]
29. Auranen M, Ylikallio E, Shcherbii M, Paetau A, Kiuru-Enari S, Toppila JP, and Tyynismaa H (2015) CHCHD10 variant p.(Gly66Val) causes axonal Charcot-Marie-Tooth disease. Neurology. Genetics 1, e1 [PubMed: 27066538]
30. Burstein SR, Valsecchi F, Kawamata H, Bourens M, Zeng R, Zuberi A, Milner TA, Cloonan SM, Lutz C, Barrientos A, and Manfredi G (2018) In vitro and in vivo studies of the ALS-FTLD protein CHCHD10 reveal novel mitochondrial topology and protein interactions. Human molecular genetics 27, 160–177 [PubMed: 29112723]
31. Genin EC, Plutino M, Bannwarth S, Villa E, Cisneros-Barroso E, Roy M, Ortega-Vila B, Fragaki K, Lespinasse F, Pinero-Martos E, Auge G, Moore D, Burte F, Lacas-Gervais S, Kageyama Y, Itoh K, Yu-Wai-Man P, Sesaki H, Ricci JE, Vives-Bauza C, and Paquis-Flucklinger V (2016) CHCHD10 mutations promote loss of mitochondrial cristae junctions with impaired mitochondrial genome maintenance and inhibition of apoptosis. Embo Mol Med 8, 58–72 [PubMed: 26666268]
32. Genin EC, Bannwarth S, Lespinasse F, Ortega-Vila B, Fragaki K, Itoh K, Villa E, Lacas-Gervais S, Jokela M, Auranen M, Ylikallio E, Mauri-Crouzet A, Tyynismaa H, Vihola A, Auge G, Cochaud C, Sesaki H, Ricci JE, Udd B, Vives-Bauza C, and Paquis-Flucklinger V (2018) Loss of MICOS complex integrity and mitochondrial damage, but not TDP-43 mitochondrial localisation, are likely associated with severity of CHCHD10-related diseases. Neurobiol Dis 119, 159–171 [PubMed: 30092269]
33. Wils H, Kleinberger G, Janssens J, Pereson S, Joris G, Cuijt I, Smits V, Ceuterick-de Groote C, Van Broeckhoven C, and Kumar-Singh S (2010) TDP-43 transgenic mice develop spastic paralysis and neuronal inclusions characteristic of ALS and frontotemporal lobar degeneration. Proc Natl Acad Sci U S A 107, 3858–3863 [PubMed: 20133711]
34. Jankowsky JL, Fadale DJ, Anderson J, Xu GM, Gonzales V, Jenkins NA, Copeland NG, Lee MK, Younkin LH, Wagner SL, Younkin SG, and Borchelt DR (2004) Mutant presenilins specifically elevate the levels of the 42 residue beta-amyloid peptide in vivo: evidence for augmentation of a 42-specific gamma secretase. Human molecular genetics 13, 159–170 [PubMed: 14645205]
35. Yoshiyama Y, Higuchi M, Zhang B, Huang SM, Iwata N, Saido TC, Maeda J, Suhara T, Trojanowski JQ, and Lee VM (2007) Synapse loss and microglial activation precede tangles in a P301S tauopathy mouse model. Neuron 53, 337–351 [PubMed: 17270732]
36. Lee MK, Stirling W, Xu Y, Xu X, Qui D, Mandir AS, Dawson TM, Copeland NG, Jenkins NA, and Price DL (2002) Human alpha-synuclein-harboring familial Parkinson's disease-linked Ala-53 --> Thr mutation causes neurodegenerative disease with alpha-synuclein aggregation in transgenic mice. Proceedings of the National Academy of Sciences of the United States of America 99, 8968–8973 [PubMed: 12084935]
37. Woo JA, Liu T, Fang CC, Cazzaro S, Kee T, LePochat P, Yrigoin K, Penn C, Zhao X, Wang X, Liggett SB, and Kang DE (2019) Activated cofilin exacerbates tau pathology by impairing tau-mediated microtubule dynamics. Commun Biol 2, 112 [PubMed: 30911686]
38. Pham AH, McCaffery JM, and Chan DC (2012) Mouse lines with photo-activatable mitochondria to study mitochondrial dynamics. Genesis 50, 833–843 [PubMed: 22821887]

39. Woo JA, Liu T, Zhao X, Trotter C, Yrigoin K, Cazzaro S, Narvaez E, Khan H, Witas R, Bukhari A, Makati K, Wang X, Dickey C, and Kang DE (2017) Enhanced tau pathology via RanBP9 and Hsp90/Hsc70 chaperone complexes. Human molecular genetics 26, 3973–3988 [PubMed: 29016855]
40. Fredriksson S, Gullberg M, Jarvius J, Olsson C, Pietras K, Gustafsdottir SM, Ostman A, and Landegren U (2002) Protein detection using proximity-dependent DNA ligation assays. Nat Biotechnol 20, 473–477 [PubMed: 11981560]
41. Anderson CJ, Bredvik K, Burstein SR, Davis C, Meadows SM, Dash J, Case L, Milner TA, Kawamata H, Zuberi A, Piersigilli A, Lutz C, and Manfredi G (2019) ALS/FTD mutant CHCHD10 mice reveal a tissue-specific toxic gain-of-function and mitochondrial stress response. Acta Neuropathol
42. Genin EC, Madji Hounoum B, Bannwarth S, Fragaki K, Lacas-Gervais S, Mauri-Crouzet A, Lespinasse F, Neveu J, Ropert B, Auge G, Cochaud C, Lefebvre-Omar C, Bigou S, Chiot A, Mochel F, Boillee S, Lobsiger CS, Bohl D, Ricci JE, and Paquis-Flucklinger V (2019) Mitochondrial defect in muscle precedes neuromuscular junction degeneration and motor neuron death in CHCHD10(S59L/+) mouse. Acta Neuropathol
43. Brockmann SJ, Freischmidt A, Oeckl P, Muller K, Ponna SK, Helferich AM, Paone C, Reinders J, Kojer K, Orth M, Jokela M, Auranen M, Udd B, Hermann A, Danzer KM, Lichtner P, Walther P, Ludolph AC, Andersen PM, Otto M, Kursula P, Just S, and Weishaupt JH (2018) CHCHD10 mutations p.R15L and p.G66V cause motoneuron disease by haploinsufficiency. Human molecular genetics 27, 706–715 [PubMed: 29315381]
44. Straub IR, Janer A, Weraarpachai W, Zinman L, Robertson J, Rogaeva E, and Shoubridge EA (2018) Loss of CHCHD10-CHCHD2 complexes required for respiration underlies the pathogenicity of a CHCHD10 mutation in ALS. Human molecular genetics 27, 178–189 [PubMed: 29121267]
45. Su C, Wang F, Ciolek D, and Pan YC (1994) Electrophoresis of proteins and protein-protein complexes in native polyacrylamide gels using a horizontal gel apparatus. Anal Biochem 223, 93–98 [PubMed: 7695108]
46. MacVicar T, and Langer T (2016) OPA1 processing in cell death and disease - the long and short of it. J Cell Sci 129, 2297–2306 [PubMed: 27189080]
47. Wai T, Garcia-Prieto J, Baker MJ, Merkwirth C, Benit P, Rustin P, Ruperez FJ, Barbas C, Ibanez B, and Langer T (2015) Imbalanced OPA1 processing and mitochondrial fragmentation cause heart failure in mice. Science 350, aad0116 [PubMed: 26785494]
48. Wu X, Li L, and Jiang H (2017) Mitochondrial inner-membrane protease Yme1 degrades outer-membrane proteins Tom22 and Om45. J Cell Biol
49. Delettre C, Griffoin JM, Kaplan J, Dollfus H, Lorenz B, Faivre L, Lenaers G, Belenguer P, and Hamel CP (2001) Mutation spectrum and splicing variants in the OPA1 gene. Hum Genet 109, 584–591 [PubMed: 11810270]
50. Huang X, Wu BP, Nguyen D, Liu YT, Marani M, Hench J, Benit P, Kozjak-Pavlovic V, Rustin P, Frank S, and Narendra DP (2019) CHCHD2 accumulates in distressed mitochondria and facilitates oligomerization of CHCHD10. Human molecular genetics 28, 349 [PubMed: 30285108]
51. Meng H, Yamashita C, Shiba-Fukushima K, Inoshita T, Funayama M, Sato S, Hatta T, Natsume T, Umitsu M, Takagi J, Imai Y, and Hattori N (2017) Loss of Parkinson's disease-associated protein CHCHD2 affects mitochondrial crista structure and destabilizes cytochrome c. Nat Commun 8, 15500 [PubMed: 28589937]
52. Purandare N, Somayajulu M, Huttemann M, Grossman LI, and Aras S (2018) The cellular stress proteins CHCHD10 and MNRR1 (CHCHD2): Partners in mitochondrial and nuclear function and dysfunction. J Biol Chem 293, 6517–6529 [PubMed: 29540477]
53. Liu W, Duan XY, Xu LN, Shang WN, Zhao JY, Wang LQ, Li JC, Chen CH, Liu JP, and Tong C (2020) Chchd2 regulates mitochondrial morphology by modulating the levels of Opa1. Cell Death Differ
54. Huynen MA, Muhlmeister M, Gotthardt K, Guerrero-Castillo S, and Brandt U (2016) Evolution and structural organization of the mitochondrial contact site (MICOS) complex and the mitochondrial intermembrane space bridging (MIB) complex. Biochim Biophys Acta 1863, 91–101 [PubMed: 26477565]

55. Darshi M, Mendiola VL, Mackey MR, Murphy AN, Koller A, Perkins GA, Ellisman MH, and Taylor SS (2011) ChChd3, an inner mitochondrial membrane protein, is essential for maintaining crista integrity and mitochondrial function. J Biol Chem 286, 2918–2932 [PubMed: 21081504]

56. Guarani V, McNeill EM, Paulo JA, Huttlin EL, Frohlich F, Gygi SP, Van Vactor D, and Harper JW (2015) QIL1 is a novel mitochondrial protein required for MICOS complex stability and cristae morphology. Elife 4

57. Aras S, Pak O, Sommer N, Finley R Jr., Huttemann M, Weissmann N, and Grossman LI (2013) Oxygen-dependent expression of cytochrome c oxidase subunit 4-2 gene expression is mediated by transcription factors RBPJ, CXXC5 and CHCHD2. Nucleic Acids Res 41, 2255–2266 [PubMed: 23303788]

58. Li Q, Yokoshi M, Okada H, and Kawahara Y (2015) The cleavage pattern of TDP-43 determines its rate of clearance and cytotoxicity. Nat Commun 6, 6183 [PubMed: 25630387]

59. Stoica R, De Vos KJ, Paillusson S, Mueller S, Sancho RM, Lau KF, Vizcay-Barrena G, Lin WL, Xu YF, Lewis J, Dickson DW, Petrucelli L, Mitchell JC, Shaw CE, and Miller CC (2014) ER-mitochondria associations are regulated by the VAPB-PTPIP51 interaction and are disrupted by ALS/FTD-associated TDP-43. Nat Commun 5, 3996 [PubMed: 24893131]

60. Colombrita C, Zennaro E, Fallini C, Weber M, Sommacal A, Buratti E, Silani V, and Ratti A (2009) TDP-43 is recruited to stress granules in conditions of oxidative insult. J Neurochem 111, 1051–1061 [PubMed: 19765185]

61. Alami NH, Smith RB, Carrasco MA, Williams LA, Winborn CS, Han SSW, Kiskinis E, Winborn B, Freibaum BD, Kanagaraj A, Clare AJ, Badders NM, Bilican B, Chaum E, Chandran S, Shaw CE, Eggan KC, Maniatis T, and Taylor JP (2014) Axonal transport of TDP-43 mRNA granules is impaired by ALS-causing mutations. Neuron 81, 536–543 [PubMed: 24507191]

62. Youle RJ, and van der Bliek AM (2012) Mitochondrial fission, fusion, and stress. Science 337, 1062–1065 [PubMed: 22936770]

63. Amati-Bonneau P, Valentino ML, Reynier P, Gallardo ME, Bornstein B, Boissiere A, Campos Y, Rivera H, de la Aleja JG, Carroccia R, Iommarini L, Labauge P, Figarella-Branger D, Marcorelles P, Furby A, Beauvais K, Letournel F, Liguori R, La Morgia C, Montagna P, Liguori M, Zanna C, Rugolo M, Cossarizza A, Wissinger B, Verny C, Schwarzenbacher R, Martin MA, Arenas J, Ayuso C, Garesse R, Lenaers G, Bonneau D, and Carelli V (2008) OPA1 mutations induce mitochondrial DNA instability and optic atrophy 'plus' phenotypes. Brain 131, 338–351 [PubMed: 18158317]

64. Joshi AU, Saw NL, Vogel H, Cunnigham AD, Shamloo M, and Mochly-Rosen D (2018) Inhibition of Drp1/Fis1 interaction slows progression of amyotrophic lateral sclerosis. Embo Mol Med 10 [PubMed: 29191946]

65. Davis SA, Itaman S, Khalid-Janney CM, Sherard JA, Dowell JA, Cairns NJ, and Gitcho MA (2018) TDP-43 interacts with mitochondrial proteins critical for mitophagy and mitochondrial dynamics. Neurosci Lett 678, 8–15 [PubMed: 29715546]

66. Lu J, Duan W, Guo Y, Jiang H, Li Z, Huang J, Hong K, and Li C (2012) Mitochondrial dysfunction in human TDP-43 transfected NSC34 cell lines and the protective effect of dimethoxy curcumin. Brain Res Bull 89, 185–190 [PubMed: 22986236]

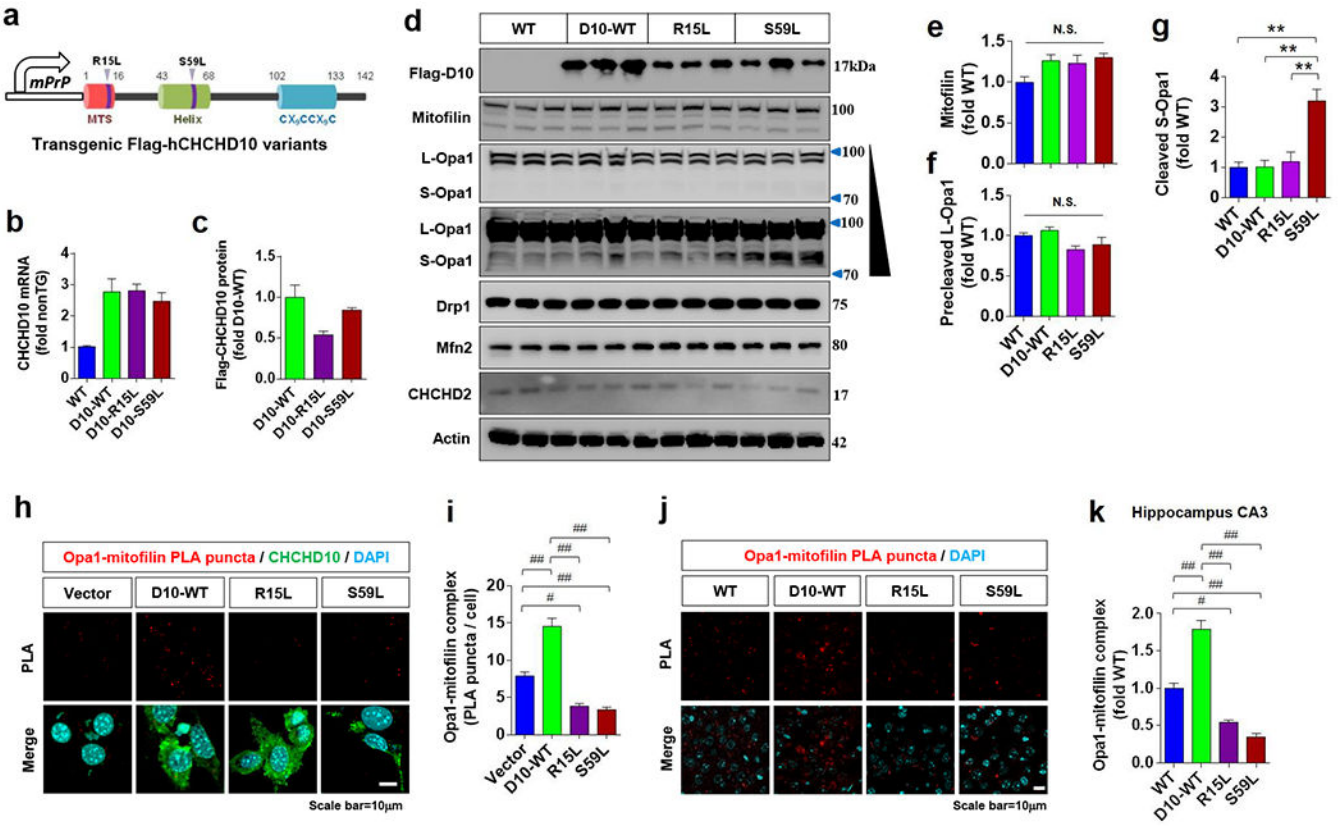

Fig. 1. FTD/ALS-linked CHCHD10 mutations disrupt OPA1-mitofilin complexes in transfected cells and *in vivo* mice

(a) Schematic model of human CHCHD10 expression (D10-WT, R15L, S59L) driven by the mouse *PrP* promoter in transgenic mice.

(b) Equal amount of total RNA isolated from the cortex of 10-month old WT and CHCHD10 transgenic mice (D10-WT, R15L, & S59L) were subjected to qRT-PCR and quantification of CHCHD10 mRNA transcripts normalized to WT (n=4 mice/genotype, average of 2 primer sets).

(c) Quantification of relative cortical Flag-hCHCHD10 protein normalized to D10-WT transgenic mice from D10-WT, R15L, and S59L transgenic mice. Flag-hCHCHD10 level was first normalized to endogenous CHCHD10 level in littermate WT mice (n=7-10 WT littermates, n=7 D10-WT, n=5 R15L, n=12 S59L).

(d) Equal protein amounts of RIPA extracts from the cortex of 10-month old WT and CHCHD10 transgenic mice (D10-WT, R15L, & S59L) were subjected to SDS-PAGE and immunoblotting for indicated proteins.

(e-g) Quantification of mitofilin and OPA1 levels (1-way ANOVA, posthoc Tukey, N.S.=not significant, **p<0.01, n=3 mice per group).

(h) NIH-3T3 cells were transfected with vector control or Flag-CHCHD10-WT, Flag-R15L, or Flag-S59L for 48h. Cells were then subjected to *in situ* proximity ligation assay (PLA) for endogenous OPA1-mitofilin complexes (red), immunostaining for Flag-CHCHD10 (green), and DAPI (blue).

(i) Quantification of PLA puncta number per cell (1-way ANOVA, posthoc Tukey, #p<0.001, ##p<0.0001, n=31/group from 4 experiments).
(j) Brain sections from 10-month old WT and CHCHD10 transgenic mice (D10-WT, R15L, & S59L) were subjected to i*n situ* PLA for OPA1-mitofilin complexes (red) and DAPI staining (blue). Representative images show hippocampus CA3 region.
(k) Quantification of PLA puncta intensity in hippocampus CA3 region (1-way ANOVA, posthoc Tukey, #p<0.001, ##p<0.0001, n=12 sections/group from 4 mice/group).

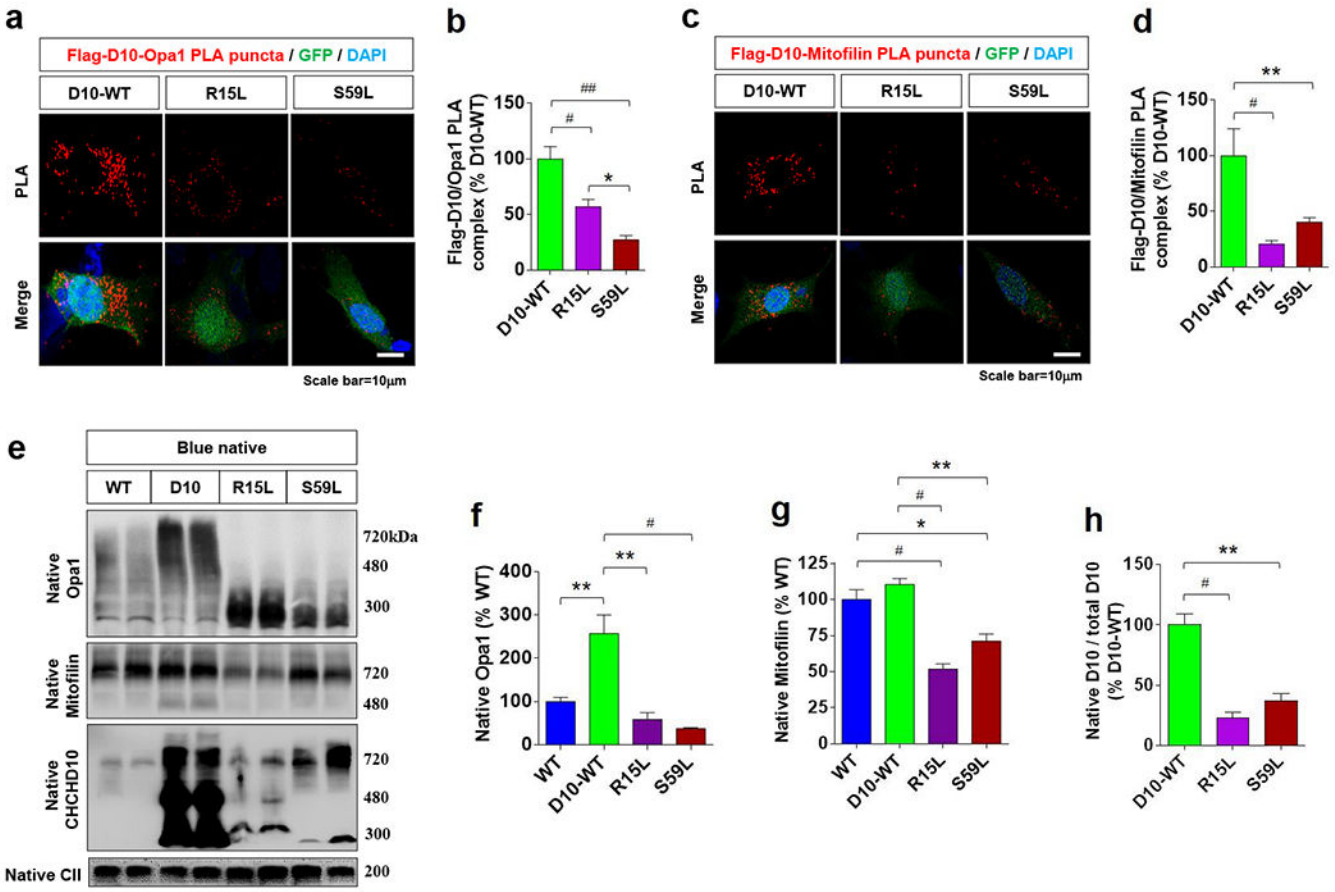

Fig. 2. FTD/ALS-linked CHCHD10 mutations exhibit reduced binding to OPA1 and mitofilin and disrupt high molecular weight native CHCHD10, mitofilin, and OPA1 *in vivo*

(a,c) NIH-3T3 cells were co-transfected with GFP and Flag-CHCHD10-WT, Flag-R15L, or Flag-S59L for 48h. Cells were then subjected to *in situ* PLA for CHCHD10-OPA1 complexes (red) or CHCHD10-mitofilin complexes (red), DAPI staining (blue), and GFP (green) fluorescence microscopy.

(b,d) Quantification of CHCHD10-OPA1 PLA intensity normalized to GFP intensity (n) and CHCHD10-mitofilin PLA intensity normalized to GFP intensity (p) (1-way ANOVA, posthoc Tukey, *p<0.05, **p<0.01 #p<0.001, ##p<0.0001, n=24–32 images/group from 4 repeat experiments).

(e) Equal protein amounts of digitonin extracts from the cortex of 10-month old WT (non-TG) and CHCHD10 transgenic mice (WT, R15L & S59L) were subjected in blue native gel electrophoresis and detection of the indicated high molecular weight (HMW) native protein complexes. Molecular weight markers in kDa are indicated to the right. Representative blots shown.

(f-h) Quantification of native OPA1, mitofilin, and CHCHD10 complexes (480–720 kDa). (1-way ANOVA, posthoc Tukey, *p<0.05, **p<0.01, #p<0.001, n=4 mice per group).

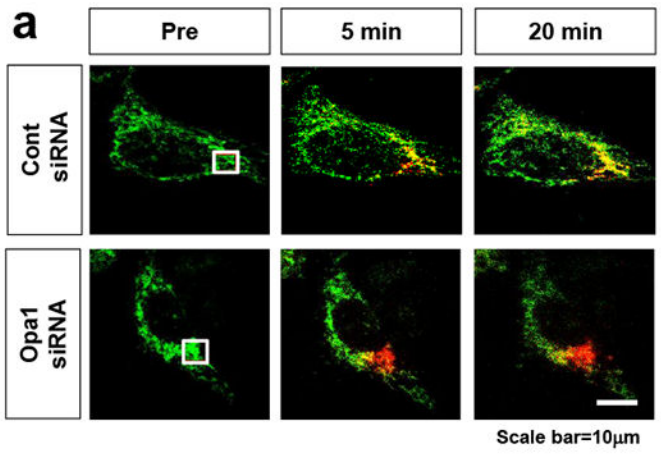

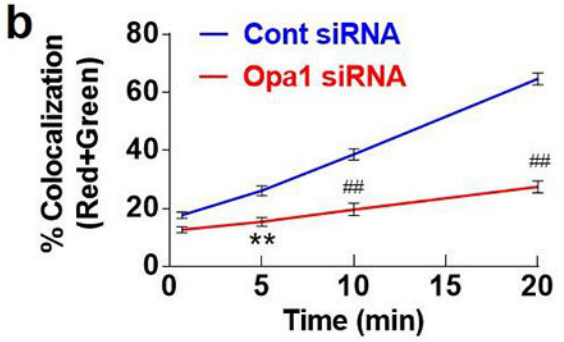

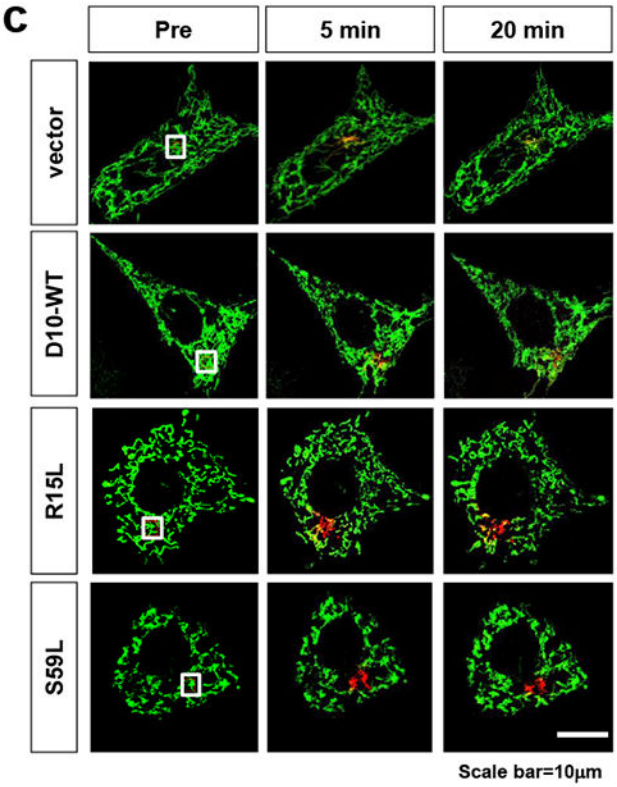

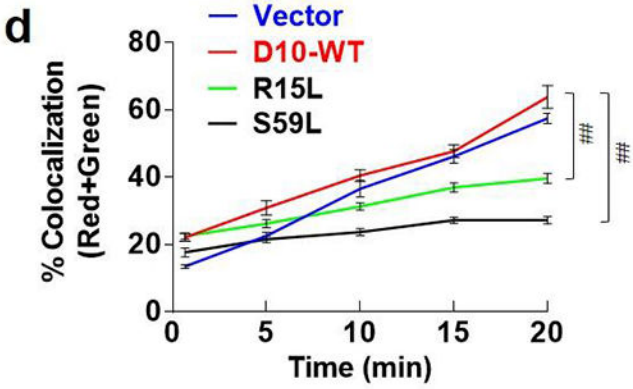

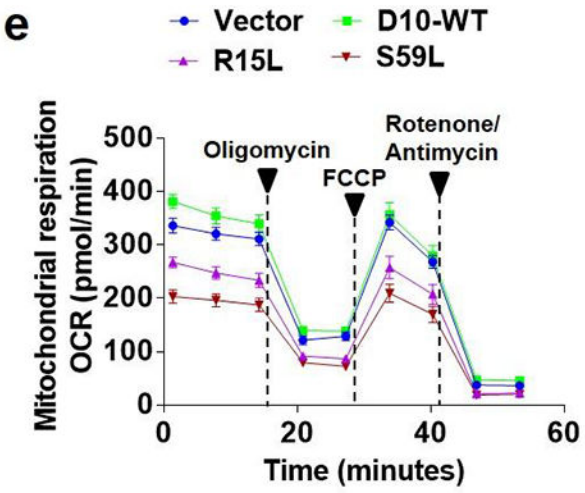

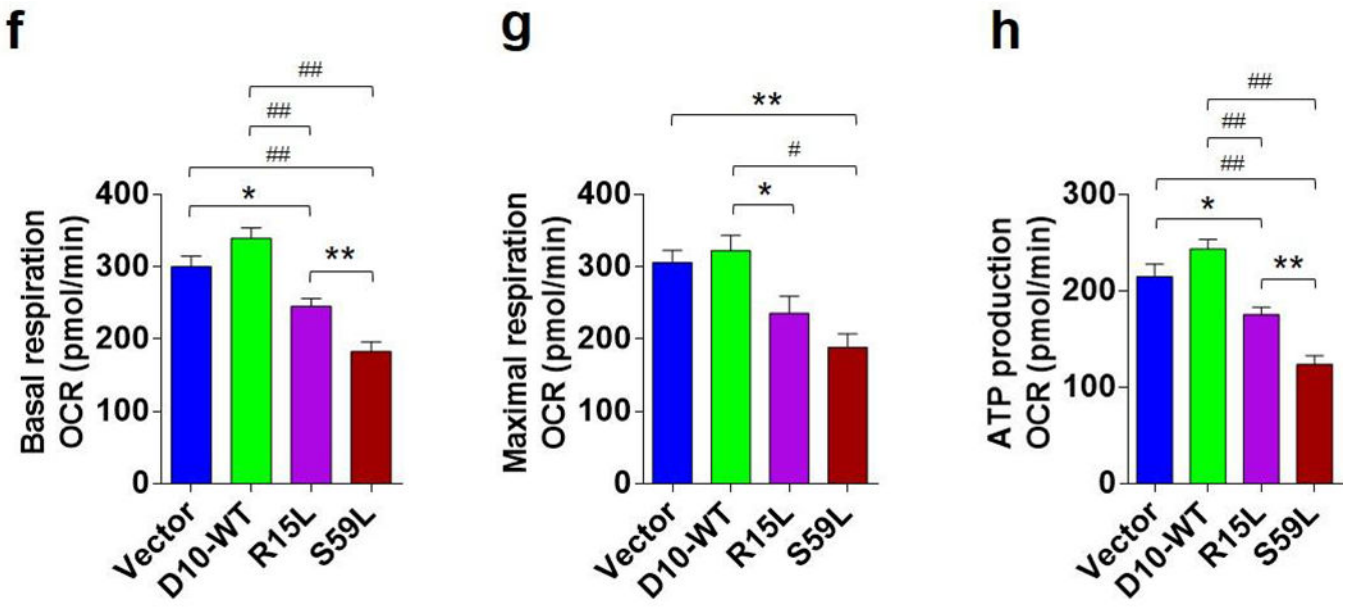

Fig. 3. FTD/ALS-linked CHCHD10 mutations impair mitochondrial fusion and respiration

(a) Hela cells were co-transfected with mito-dendra2 and control siRNA or OPA1 siRNA for 72h and subjected to photoconversion of mito-dendra2 at 405nm followed by live cell imaging over a 20 minutes period. Pre=pre-photoconversion. While boxes show photoconverted ROIs. Representative images shown.

(b) Quantification of the percentage of red/green colocalization in ROI (2-way ANOVA, posthoc Sidak, **p<0.01 #p<0.001, ##p<0.0001, n=3 repeats).

(c) NIH-3T3 cells were co-transfected with mito-dendra2 and vector control, CHCHD10-WT, R15L, or S59L for 48h and subjected to photoconversion of mito-dendra2 at 405nm followed by live cell imaging over 20 minutes period. Pre=pre-photoconversion. While boxes show photoconverted ROIs. Representative images shown.

(d) Quantification of the percentage of red/green colocalization in ROI (2-way ANOVA, posthoc Sidak, ##p<0.0001 at 10-20 minutes time points, n=10 cells/group from 3 repeat experiments).

(e) HEK293T cells were transfected pcDNA vector control or CHCHD10 variants (WT, R15L, or S59L) for 24h and allowed to grow in low serum medium (2% FBS) for 24h. Equal number of cells were then subjected to mitochondrial respiration assay using XF96 Seahorse (mito stress test) with injection of the indicated drugs at indicated time points. Graph shows average of 3 experiments.

(f-h) Quantification of basal respiration, maximal respiration, and ATP production phases of OCR (1-way ANOVA, posthoc Tukey, *p<0.05, **p<0.01, #p<0.001, ##p<0.0001, n=22–27 measurements/group from 3 repeat experiments).

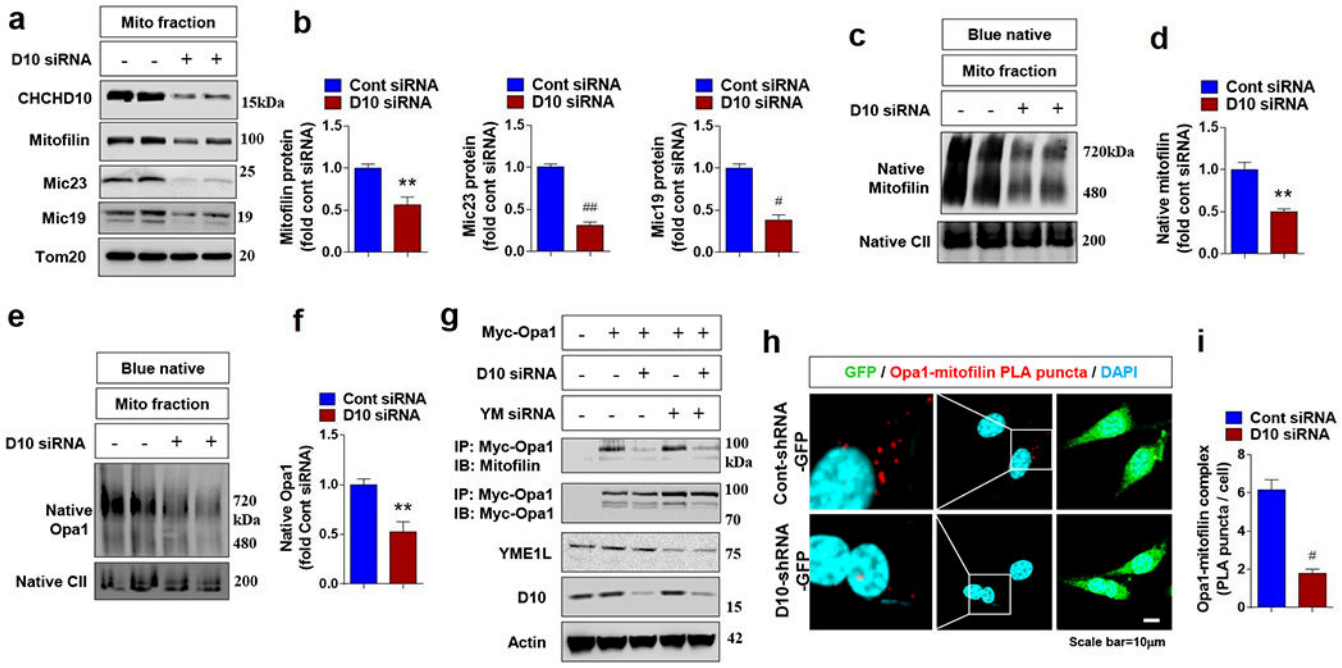

Fig. 4. Knockdown of endogenous CHCHD10 destabilizes MICOS components and OPA1-mitofilin interaction

(a) HEK293T cells were transfected with control siRNA or CHCHD10 siRNA for 72h and subjected to mitochondrial isolation. Equal protein amounts of mitochondrial lysates were then subjected to SDS-PAGE and immunoblotting for indicated proteins. Representative blots shown.

(b) Quantification of mitofilin, Mic23 and Mic19 (t-test, **p<0.01, #p<0.001, ##p<0.0001, n=4/group).

(c,e) HEK293T cells were transfected with control and CHCHD10 siRNA for 72h and subjected to mitochondrial isolation. Equal protein amounts of digitonin extracted mitochondria were then subjected to blue native gel electrophoresis and detection of high molecular weight native bands containing mitofilin (c) or OPA1 (e) as well as native Complex II as loading control. Molecular weight markers in kDa are indicated to the right. Representative blots shown.

(d,f) Quantification of 480-720 kDa native mitofilin (d) or native OPA1 (f) bands (t-test, **p<0.01, n=4/group).

(g) HEK293T cells were transfected with vector control or myc-OPA1 and control siRNA, CHCHD10 siRNA and/or YME1L siRNA for 72h. Equal protein amounts of whole cell lysates were then subjected to immunoprecipation (IP) using anti-myc antibody and immunoblotting for mitofilin and myc-OPA1 or direct immunoblotting for indicated proteins.

(h) NIH3T3 cells were transduced with control shRNA-GFP lentivirus or CHCHD10 shRNA-GFP lentivirus for 60h and subjected to *in situ* PLA for OPA1-mitofilin complexes (red), DAPI staining (blue), and GFP fluorescence (green). Representative images shown.

(i) Quantification of OPA1-mitofilin complex PLA puncta per cell (t-test, #p<0.001, n=19–38 images from 4 repeat experiments).

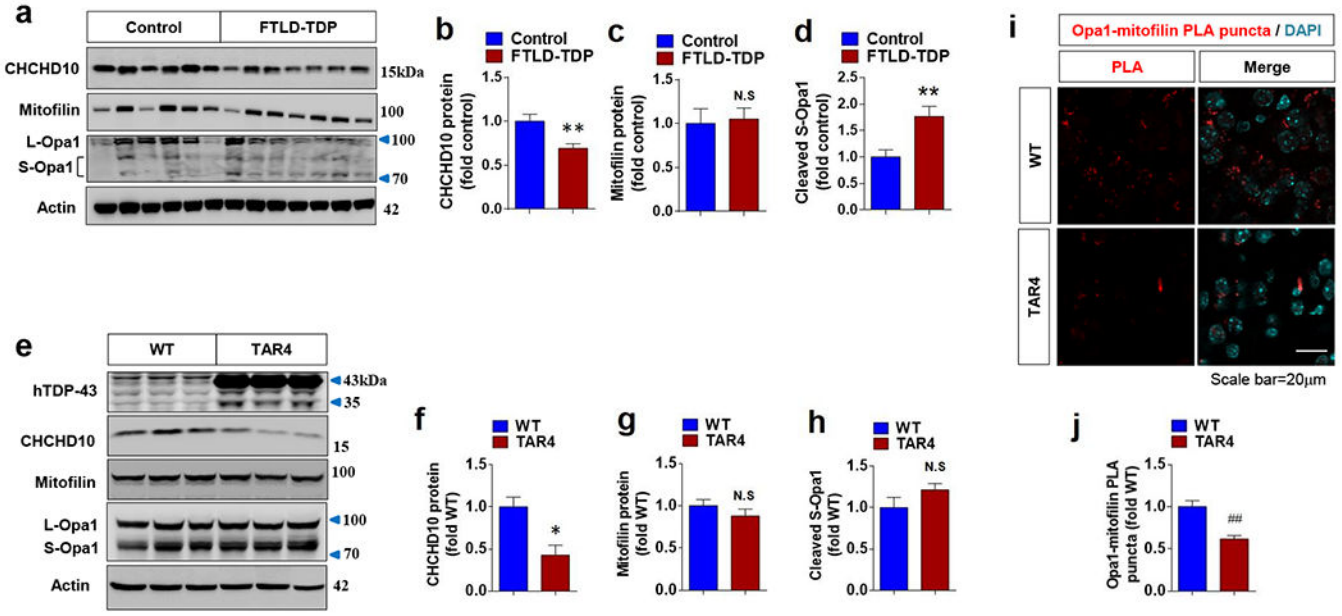

Fig. 5. Reduced CHCHD10 and OPA1-mitofilin complex in brains of FTLD-TDP and TDP-43 transgenic mice

(a) Equal protein amounts of RIPA extracts prepared from the frontal gyri of post-mortem pathology confirmed FTLD-TDP and nondemented control cases were subjected to immunoblotting for CHCHD10, mitofilin, OPA1, and actin. Representative blots shown.

(b-d) Quantification of CHCHD10, mitofilin and cleaved S-OPA1 (~75-85 kDa) proteins from RIPA extracts (t-test, **p<0.01, n=13 control, n=10 FTLD-TDP).

(e) Equal protein amounts of RIPA extracts from the cortex of 18-month old hTDP-43 transgenic (TAR4) and WT littermate mice were subjected to immunoblotting for human TDP-43 (hTDP-43), CHCHD10, mitofilin, OPA1, and actin.

(f-h) Quantification of CHCHD10, mitofilin and cleaved S-OPA1 (~75-80 kDa) from TAR4 and WT littermate cortex (t-test, **p<0.01, n=3 mice/per group).

(i) Brain sections from 18-month-old TAR4 transgenic and WT littermate mice were subjected to *in situ* PLA for OPA1-mitofilin complexes (red) and DAPI staining (blue). Representative images show the frontal cortex.

(j) Quantification of PLA puncta intensity in the frontal cortex (t-test, ##p<0.0001, n=22 images/group from 4 mice/group).

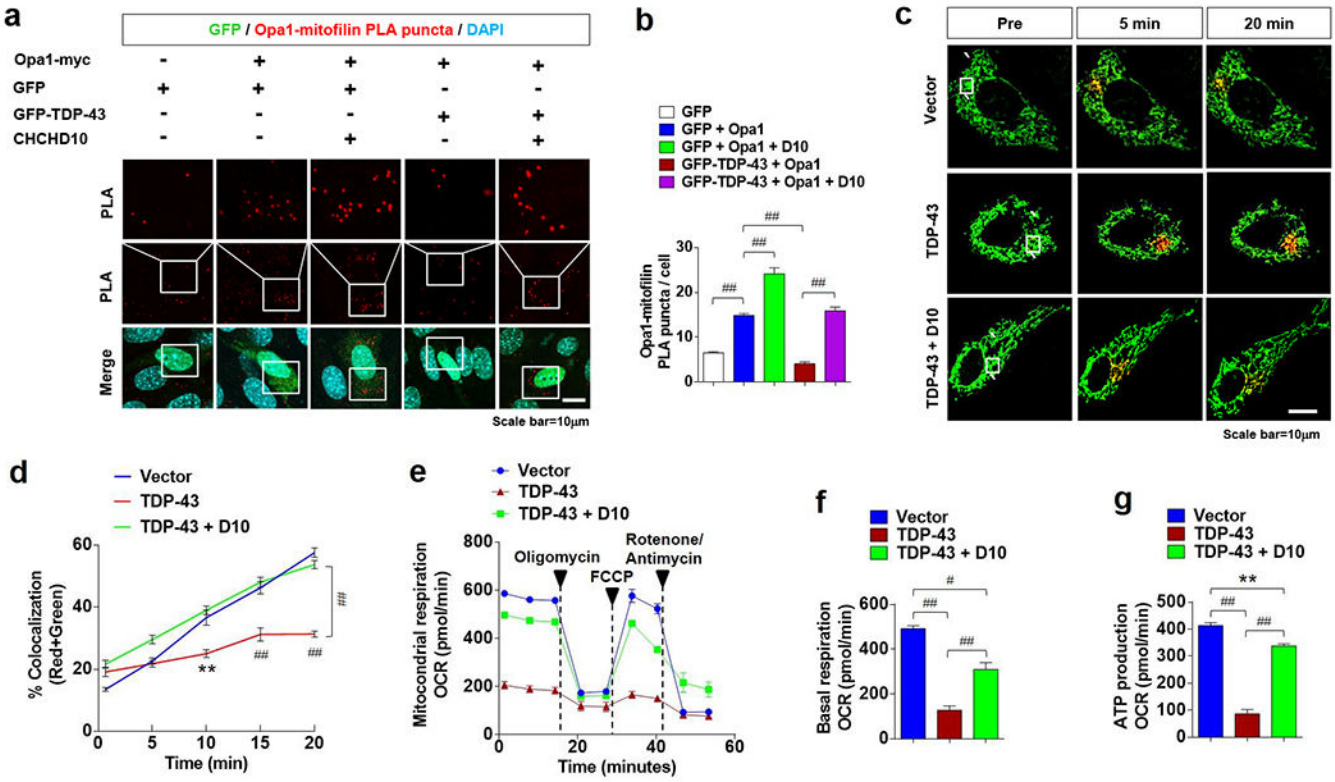

Fig. 6. TDP-43 recapitulates mitochondrial abnormalities associated with CHCHD10 mutations and are rescued by wild type CHCHD10

(a) NIH3T3 cells were co-transfected with GFP or GFP-TDP-43 ± OPA1-myc and/or CHCHD10-WT for 48h. Cells were then subjected to *in situ* PLA for OPA1-mitofilin complexes (red), DAPI staining (blue), and GFP fluorescence (green). White box regions magnified in upper panels.

(b) Quantification of OPA1-mitofilin PLA puncta per cell (1-way ANOVA, posthoc Tukey, ##p<0.0001, n=18-23 images from 3 repeat experiments).

(c) NIH3T3 cells were co-transfected with mito-dendra2 and pcDNA vector control, TDP-43, or TDP-43+CHCHD10-WT for 48h. Transfected cells were then subjected to photoconversion of mito-dendra2 at 405nm followed by live cell imaging over a 20 minutes period. Pre=pre-photoconversion. White boxes show photoconverted ROIs. Representative images shown.

(d) Quantification of percentage of the red/green colocalization in ROI (1-way ANOVA, posthoc Tukey, **p<0.01 #p<0.001, ##p<0.0001, n=10 cells/group from 3 repeat experiments).

(e) HEK293T cells were transfected with pcDNA vector control, TDP-43, or TDP-43+ CHCHD10-WT for 24h and starved in low serum medium (2% FBS) for 24h. Cells were then subjected to mitochondrial respiration assay (mito stress test) using Seahorse XFe96 instrument to measure oxygen rate consumption (OCR) with the indicated drug treatments at indicated time points.

(f,g) Quantification of basal respiration and ATP production phases of OCR (1-way ANOVA, posthoc Tukey, **p<0.01, #p<0.001, ##p<0.0001, n=9 measurements/group from 3 repeat experiments).

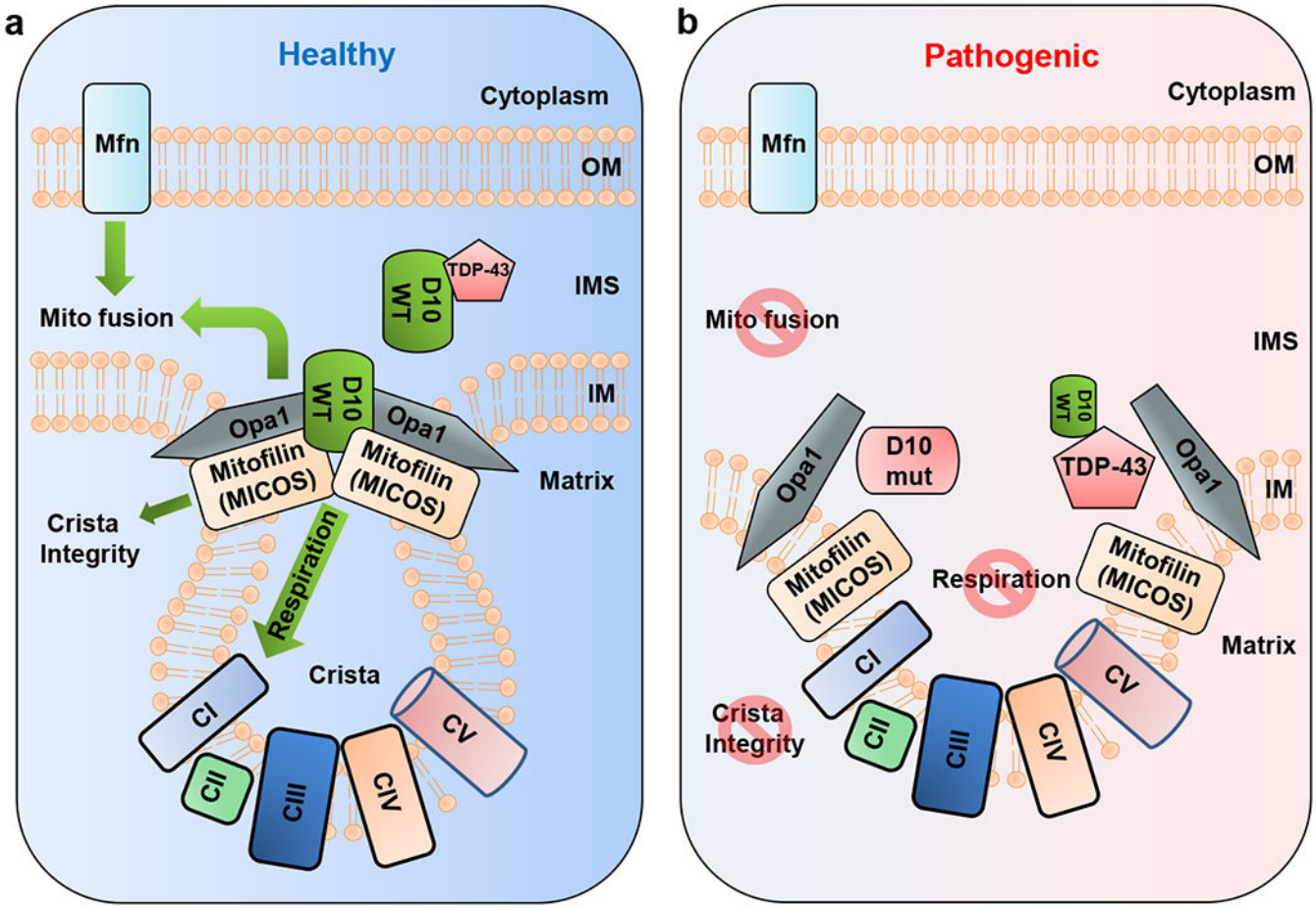

Fig 7. CHCHD10 and TDP-43 mediated coordination of mitochondrial fusion, respiration, and cristae integrity in healthy or pathogenic conditions

(a) In mitochondria of healthy brains, WT CHCHD10 interacts with both OPA1 and mitofilin/MICOS complexes and promotes OPA1-mitofilin interactions, which stabilizes both OPA1 and mitofilin complexes. Stabilization of the native OPA1 complex and OPA1-mitofilin interaction tips the balance of mitochondrial dynamics toward fusion. Stabilization of mitofilin/MICOS complex promotes the maintenance of cristae integrity and facilitates the activity of mitochondrial respiratory complexes (CI-CV). At the same time, healthy expression of WT CHCHD10 counteracts TDP-43-induced disruption of OPA1-mitofilin complexes.

(b) In mitochondria of pathogenic brains (i.e. FTLD-TDP), either CHCHD10 mutations (i.e. R15L or S59L) or TDP-43 disrupt both native OPA1 and mitofilin complexes as well as OPA1-mitofilin interaction by interfering with the ability of CHCHD10 to stabilize OPA1-mitofilin complexes. This inhibits mitochondrial fusion, tipping the balance toward fission. Disruption of mitofilin/MICOS complexes leads to impaired cristae integrity and defective activity of mitochondrial respiratory complexes (CI-CV).